DEVELOPMENT OF IMPROVED GALLIUM ARSENIDE SOLAR CELLS

Final Report

Period Covered

29 June 1964 through 28 February 1965

Prepared for:

NATIONAL AERONAUTICS & SPACE ADMINISTRATION
Goddard Space Flight Center
Greenbelt, Maryland

Contract NAS5-9006

Prepared by:

RADIO CORPORATION OF AMERICA
Special Electronic Components Division
Direct Energy Conversion Department
Mountaintop, Pennsylvania

DEVELOPMENT OF IMPROVED GALLIUM ARSENIDE SOLAR CELLS

Final Report

Period Covered

29 June 1964 through 28 February 1965

Prepared for:

NATIONAL AERONAUTICS & SPACE ADMINISTRATION
Goddard Space Flight Center
Greenbelt, Maryland

Contract NAS5-9006

Prepared by:

RADIO CORPORATION OF AMERICA
Special Electronic Components Division
Direct Energy Conversion Department
Mountaintop, Pennsylvania

TABLE OF CONTENTS

		Page
I.	INTRODUCTION	1
	A. History	1
	B. Scope	2
	C. Accomplishments	2
II.	DISCUSSION	2
	A. Manufacturing Process	2
	B. Description of the Device	6
	C. Fabrication Investigations and Results	6
	D. Measurements with Respect to Contacts, Material & Temperature Contacts	15
	E. High Temperature Storage Testing	36
III.	CONCLUSIONS AND RECOMMENDATIONS	42
	APPENDIX A	45

LIST OF FIGURES

No.		Page
1	GaAs Solar Cell	7
2	GaAs Solar Cell Relative Spectral Response Versus Wavelength for Different Diffusion Times	10
3	V-I Characteristics During Optimization Etch Step With Corresponding Sheet Resistances	12
4	GaAs Solar Cell Relative Spectral Response Vs. Wavelength With Curves Corresponding to Those of Fig. 1	13
5	Cell Efficiency Correlation with Shunt Resistance	18
6	Oscillation Period of Reverse Bias Transient Versus Base Resistivity	19
7	Reflectance Characteristics of GaAs and Silicon Monoxide Coated GaAs	24
8	Optical Transmission Curves of GaAs and Zinc Diffused GaAs	26
9	Optical Transmission Curves of GaAs and Zinc Diffused GaAs	27
10	Current Voltage Characteristics Versus Temperature	28
11	Graph of Voltage Vs. Temperature for a Gallium Arsenide Solar Cell	29
12	Graph of Voltage Vs. Temperature for a 2 x 2 cm Silicon Solar Cell	30
13	Graph of Current Vs. Temperature for a Gallium Arsenide Solar Cell	31

LIST OF FIGURES (CONT'D.)

No.		Page
14	Graph of Temperature Vs. Efficiency and Maximum Power of 1 x 2 cm Gallium Arsenide Solar Cell	32
15	Graph of Temperature Vs. Efficiency and Maximum Power of a 2 x 2 cm Silicon Solar Cell	33
16	Graph of Efficiency of GaAs and Si Solar Cells at Today's Potential Best Efficiency for Tungsten	34
17	Efficiency Ratio Versus Temperature	35
18	Temperature Vs. Spectral Response	37
19	Spectral Response Before and After 137 Hours of Storage at 200°C	43

LIST OF TABLES

No.		Page
I	Physical Properties of GaAs and Si	8
II	Diffusion Parameters Vs. Short Circuit Current	9
III	Resistance-Capacitance and Current-Voltage Distributions for Gallium Arsenide Cells Having Nickel:Silver Contacts	16
IV	Spectral Half-Peak Band Width Correlation With Cell Performance	16
V	Resistance-Capacitance and Performance Characteristics for Tin:Silver Gallium Arsenide Cells Having Tin:Silver Contact Cells	17
VI	Measured Oscillation Period of Reserve Bias Transient and Efficiencies of Gallium Arsenide Solar Cells	21
VII	Concentrations of Major Impurities in Gallium Arsenide	22
VIII	Correlation of Impurities to the Arsenic to Gallium Ratio	23
IX	Parameter Change at 200°C Storage Temp. Ti-Ag Front and Back Contacts	38
X	Parameter Change at 250°C Storage Temp. Ti-Ag Front and Back Contacts	38

LIST OF TABLES (CONT'D.)

No.		Page
XI	Parameter Change at 200°C Storage Temp. Ti-Ag Front and Sn-Ag Back Contacts	39
XII	Parameter Change at 250°C Storage Temp. Ti-Ag Front and Sn-Ag Back Contacts	39
XIII	Parameter Change at 250°C Storage Temperature	40
XIV	Parameter Change of Cells Having Sn-Ag Back and Ti-Ag Front Contacts	41
XV	Percentage of Spectral Response Loss After 137 Hours of Storage	

DEVELOPMENT OF IMPROVED GALLIUM ARSENIDE SOLAR CELLS

Contract NAS5-9006
Final Report

I. INTRODUCTION

A. History

Interest in gallium arsenide solar cells was first aroused in 1955 when a theoretical study by D. A. Jenny, J. J. Loferski, and P. Rappaport at the RCA Laboratories at Princeton, N. J. showed gallium arsenide to have the proper bandgap for optimum match of the solar spectrum. This meant that gallium arsenide would yield the highest theoretical conversion efficiency of any common semiconductor material. Because of this strong potential, work on fabrication of these cells began at the RCA Laboratories in 1956 under RCA and U. S. Signal Corps sponsorship (Contract No. DA-36-039-SC-78184). Despite the fact that the first program was severly limited by crystal size and quality, it was clearly demonstrated that gallium arsenide solar cells could be made.

In 1959, the Semiconductor and Materials Division (now the Electronic-Components and Devices Division) of RCA at Somerville, N. J. undertook a research and development program on gallium arsenide solar cells under Air Force Contract No. AF33(616)-6615. Using the technology established at the RCA Laboratories, as a basis, rapid progress was made. The first cells had efficiencies of three and four percent and were extremely small in size. The efficiency and size of the cells improved steadily and rapidly and in 1962 a more extensive program was begun under Air Force Contract No. AF33-(657)-8921. This program produced jigs, fixtures and processes for the fabrication of cells on a small pilot line basis. The crystal growing process was improved such that an increase in the quality and size of the material was realized. Efficiencies of eight to eleven percent were obtained routinely.

In 1964 the device facilities were transferred to the RCA Electronic-Components and Devices Division at Mountaintop, Pa. in order to better take advantage of the process and technology existing in the silicon solar cell development and production facilities at that location. In July of 1964 work was started on the present contract NAS5-9006.

B. Scope

The objectives of this contract were to develop a contacting mechanism having a low series resistance and high bonding strength, to better understand and improve the high temperature characteristics and reliability, and to accumulate data relating junction characteristics to electrical results.

The overall general purpose for the program was to fabricate gallium arsenide solar cells which would have a possible application in high temperature space missions where silicon solar cells would no longer be useful.

C. Accomplishments

After trying Ni-Ag contacts as used at RCA Somerville in fabricating cells under the Air Force contract, Ti-Ag as used by RCA Mountaintop in fabricating silicon solar cells, and Sn-Ni-Ag as used by RCA Laboratories in fabricating gallium arsenide lasers, a final contact mechanism of Ti-Ag "P" and Sn-Ag "N" was decided upon. This mechanism produces cells having a series resistance of less than .5 ohms and a "P" contact strength exceeding 300 grams and an "N" contact strength exceeding 1000 grams.

Although the problem of degradation at high temperatures was not solved, much information was gained concerning the cause of degradation and the area of concern was reduced to the surface of the solar cell.

The junction characteristic data obtained indicates a deficiency in processing and/or material. The data also shows significant gains are achieved by using the above mentioned contacting mechanism.

II. DISCUSSION

A. Manufacturing Process

The process for fabrication of gallium arsenide solar cells, to which the most recent state-of-the-art cells were made, is presented below. The reader is referred to the Final Report on Air Force Contract No. 33(657)-8921 for illustrations of the equipment used.

1. Material Preparation

The material used in this program was provided by the crystal growing facilities at RCA Somerville, N. J. The gallium arsenide

is a single crystal cut on the 1:1:1 plane and doped with Ge to a concentration of 5×10^{15} to 2×10^{16} #/cc. The material is sliced into wafers and both side mechanically lapped to a thickness of .020" before shipment to Mountaintop. After receiving the wafers (still in the "bread loaf" shape typical of the gradient freeze growing process), the lapping residue is removed by spraying with Cobehm (triple distilled chloroform) and wiping with cotton swabs dipped in trichlorethylene.

2. Chemical Polishing

The wafers are chemically polished to remove the work damage caused by lapping. They are then placed in a polyethylene container with the $<\bar{1}:\bar{1}:\bar{1}>$ (As) side facing up. Prior to the slicing operation the crystal is notched such that when viewing the As side of the wafer the notch would appear in the upper left hand corner. The wafers are then etched in a 5:1 solution of H_2O_2 (30% unstabilized):HF(49%) for 5 min. This removes approximately .003" to .004" of material from the top surface. There is no significant removal from the back surface. The wafers are then flushed with DI water for 3 min. after which they are covered with HF for 2 min. and once again rinsed with DI water for 5 min. They are then blown dry using filtered dry air.

3. Chromic Acid Treatment

An oxide is formed on the surface in order to better control the Zn diffusion. This is accomplished by placing the wafers in petri dishes (once again the As side facing up) and covering them with chromic acid. The dishes are then placed on a hot plate and maintained at a temperature of $90^{o}C$ for 1 hour. They are then removed, rinsed in DI water for 5 min., and blown dry using filtered dry air.

4. Diffusion

Prior to diffusion the source material (40% Zn: 60% In) is cleaned in a 1:9 HCl:H_2O solution for 2 min., rinsed in DI water, rinsed in acetone and blown dry. The quartz parts are cleaned in a 5:15:2 HNO3:HCl:HF solution for 30 min., rinsed in DI water and blown dry.

The box type diffusion is accomplished in a conventional wire wound furnace (see First Quarterly Progress Report for description of box diffusion boat). The diffusion is carried out at

720°C for 10 min. in an ambient atmosphere of "90-10" forming gas.

This diffusion process produces a junction depth between 1.5 and 2.0 microns and a sheet resistance between 15 and 45 ohms/□. The junction depth is measured using the cylindrical groove technique and the sheet resistance is determined with a conventional four-point probe.

5. Wax Mounting

Using a rosin-beeswax composition, wafers are mounted on a glass microscope slide such that the back or Ga side is exposed. The wafers are positioned such that they are properly indexed for the ultrasonic cutting operation.

6. Ultrasonic Cutting

1 x 2 cm wafers are ultrasonically cut out of the "bread loaf" wafer. An ultrasonic impact grinder with a 1 x 2 cm tool is used in this operation. Number 600 grit abrasive and water is used for the slurry. It should be noted that although the # "P" type layer is eliminated from the edges of the 1 x 2 cm wafer there is quite a bit of work damage done to the junction at the wafers edge. This could very easily cause "slump" in the knee of the voltage-current curves. It is recommended that future work include starting with a 1 x 2 cm wafer such that the work damage at the edges can be removed during chemical polishing.

7. Back Etching

The "P" layer on the back of the wafer is etched off before the wafer is removed from the glass slide. The slide and wafer are immersed in a 5:1 H_2O_2:HF solution for 1 min., rinsed under DI water and blown dry.

8. Demounting and Cleaning

The slides are placed in a beaker of hot stabilized trichloreythlene. The combination of heat and solvent action cause the wafer to slide off the glass slide. The wafers are then thoroughly washed in three consecutive hot trichlorethylene rinses followed by a hot unstabilized trichlorethylene rinse.

9. Pre-evaporation Cleaning

In order to remove the oxide formed during the chromic acid treatment, the wafers are hydrogen fired at 610°C for 5 min. This operation takes place in a belt furnace immediately prior to contact evaporation.

10. Contact Evaporation

The wafers are placed in the evaporation jigs and then into the evaporator. The back ("N") contact is applied first. The front ("P") is shielded such that it is protected from silver flash over. Five-tenths of a gram of Sn are evaporated from a throw distance of 14-1/2 inches from the substrates. Seven grams of Ag are then evaporated at a throw distance of 13-1/2 inches. The bell jar is back filled with N2 to break the vacuum. The jigs are then turned over in preparation for the application of the "P" Ti-Ag contact. The Ti is monitored by resistance measurements on a glass slide having an exposed area of 1-1/2 inches^2. The Ti is evaporated at a throw distance of 14-1/2 inches until the resistance of the slide is 500 Ω. The Ag is then blended with the Ti until a negligible resistance is observed after which the remainder of the 7 grams of Ag is evaporated at a throw distance of 13-1/2 inches. Once again N_2 is used to break the vacuum.

11. Sintering

The contacts are sintered by H2 firing at 610°C for 5 minutes in a belt furnace.

12. Optimization Etching

The junction must be diffused relatively deep so that the front contacts do not penetrate to the "N" side and cause shorting. In order to increase the spectral response and the conversion efficiency, the surface must be removed to within approximately .5 microns from the junction. The solution used for this etch consists of KOH (25%) and H_2O_2 (30%). The volumetric ratio is 10:1. A light source is used and the cells are etched for numerous increments of time with V-I curves being taken after each increment until the optimized V-I curve is achieved. The total etching time is normally 1 to 3 minutes depending on the diffusion conditions.

13. Anti-reflective Coating

An anti-reflection coating of SiO is evaporated onto the surface of the device. The thickness of approximately 800Å is monitored by eye. This operation results in a 15 to 30% increase in cell efficiency.

14. Electrical Testing

V-I curves are taken on all cells. The 2800°K tungsten light source is adjusted to an intensity of 100 mw/cm^2 by using cells calibrated at Table Mountain, Calif. There is a 3 cm. deep DI water filter between the light source and the cell.

B. Description of the Device

1. Physical Dimensions

The weight of the cell in finished form is approximately 42 milligrams. All dimensions are nominal (see Fig. 1).

2. Physical Properties of GaAs and Si

Physical properties of GaAs and Si cells are listed in Table I on page 8.

C. Fabrication Investigations and Results

1. Diffusion

Keeping the temperature at 720°C, various diffusion times were investigated which would provide good electrical units. The time of 10 minutes was chosen as the minimum. This time produced junction depths of 1.5 to 2.0 microns. Times less than 10 minutes (actually junctions less than 1.5 microns) would produce cells having a low V_{OC} indicating a low shunting resistance across the junction.

Several diffusion experiments were conducted to determine the dependency of the collection efficiency on the diffused impurity profile. Diffusions made at twice the normal time (at the normal temperature) produced a maximum short-circuit current (after etching) of 15 ma. Diffusions made at the normal time and 30% less than the normal time (at temp. 25°C above the

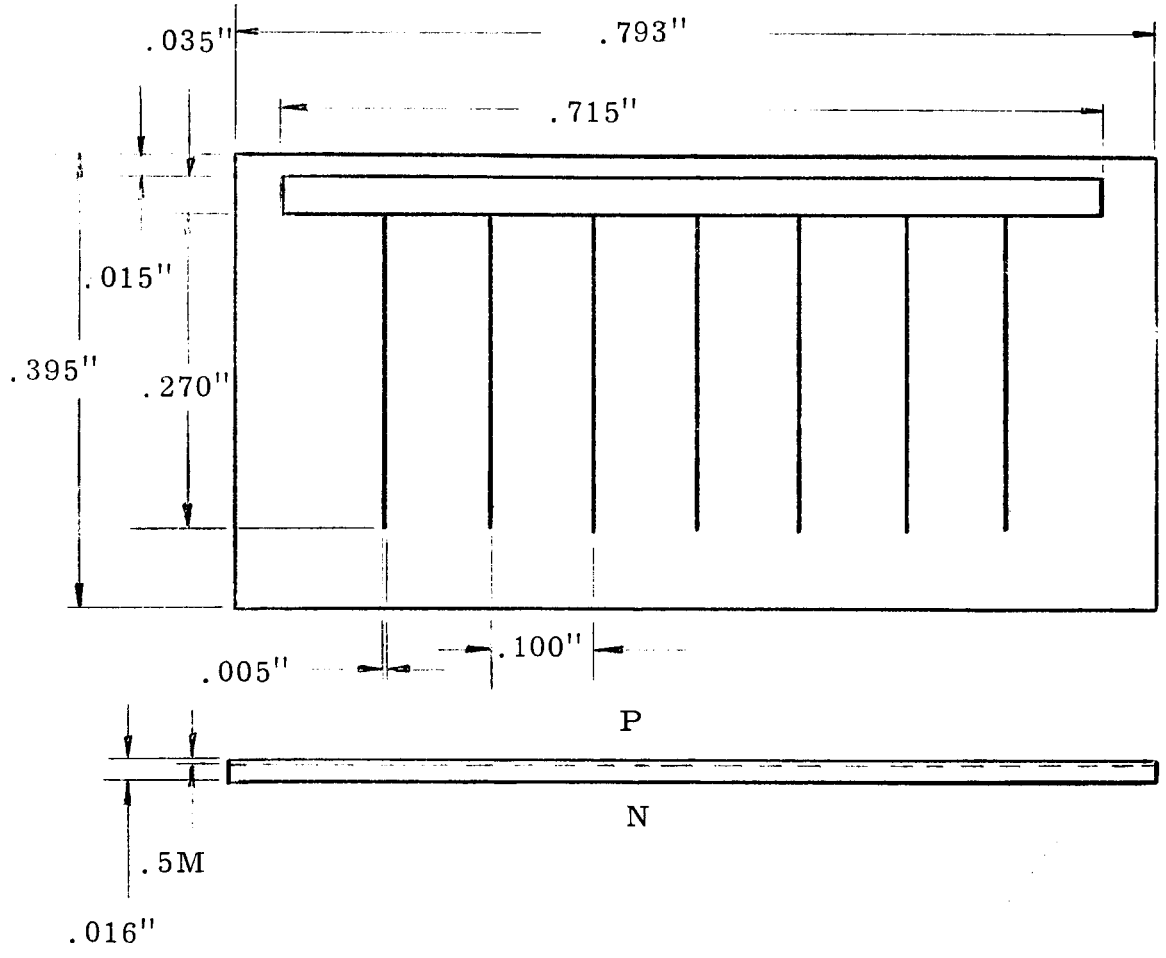

Fig. 1. GaAs Solar Cell

Table I

Physical Properties of GaAs and Si

Properties	Si	GaAs
Melting Point (^{o}C)	1420	1238
Density (g/cm^3)	2.328	5.312
Liquid Density (g/cm^3 at M.P.)		5.45
Lattice Constant (A^{o})	5.431	5.654
Dist. Betw. Nearest Neighbors (Å)	2.35	2.45
Atoms per cm^3 (x 10^{22})	4.99	4.43
Thermal Coeff. of Expansion (/^{o})	4.2×10^{-6}	5.93×10^{-6}
Pressure at M.P. (atm)	10^{-6}	0.9
Thermal Conductivity (watt units)	.84	0.52
Specific Heat (cal/gm)	.181	0.086
Latent Heat of Fusion (kcal/mole)	9.45	21 ± 3
Dielectric Constant	11.7	11.1
Elastic Moduli C_{11}	1.674	1.188
(x 10^{12} dynes/cm2) C_{12}	.652	0.538
C_{44}	.796	0.594
Volume compressibility (x10^{-12} cm2/degree)	.98	
Magnetic Susceptibility (cgs)	$-.13 \times 10^{-6}$	
Debye Temperature (^{o}K)	652	
Emissivity (1200^{o}C)	$\sim$ .5	
Band Gap (25^{o}C)	1.106	1.40
Temp. Dep. of Band Gap (ev/^{o}C)	-4.4×10^{-4}	-4.5×10^{-4}
Electron Lattice Mobility (cm2/v-sec)	1900	12,000
Hole Lattice Mobility	425	450
Temp. Dep. Electron Lattice Mobility	T-2.5	$\sim$T-1
Temp. Dep. Hole Lattice Mobility	T-2.7	T-2.1
Electron Effective Mass Ratio	1.1	.072
Hole Effective Mass Ratio	0.59	0.5
Intrinsic Electrons (25^{o}C) (cm^{-3})	1.5×10^{10}	1.4×10^{6}
Intrinsic Resistivity (25^{o}) (ohm-cm)	2.3×10^{5}	3.7×10^{8}

normal temperature) produced a maximum short circuit current of 19 ma. Normal time and temperature diffusions (10 min. at 720°C) produced a maximum short circuit current of 25 ma. Table II summarizes the results.

Table II

Diffusion Parameters Vs. Short Circuit Current

Diffusion Temperature	Diffusion Time	Max. Optimized Short Circuit Current
N	2N	15 ma
N + 25°C	N; N-30%	19 ma
N	N	25 ma

N = normal processing time or temperature.

From the above it was concluded that the collection efficiency is very sensitive to changes in the shape of the impurity profile of the diffused region.

Extremely short diffusions were made to further investigate the above. Keeping the normal temperature of 720°C, diffusions were made using a time of one minute. The electrical characteristics of these cells were poor; however, Fig. 2 illustrates the decided increase in spectral response over the normally diffused cell.

The main conclusion to be made concerning the above information is that a significant increase in conversion efficiency is possible if the problems of making shallow uniform junctions and contacting to them can be solved.

2. Evaporation

At the beginning of the program an evaporated layer of Ni followed by an evaporated layer of Ag was used as the contacting mechanism for both the "P" and the "N" side of the device. Using this mechanism, the series resistance of the device was in the 3-4 ohm range. Several cells were fabricated using the same Ti-Ag mechanism used on Si solar cells. The Ti-Ag seemed slightly better, however, the series resistance was still in the 3-4 ohm range. Further investi-

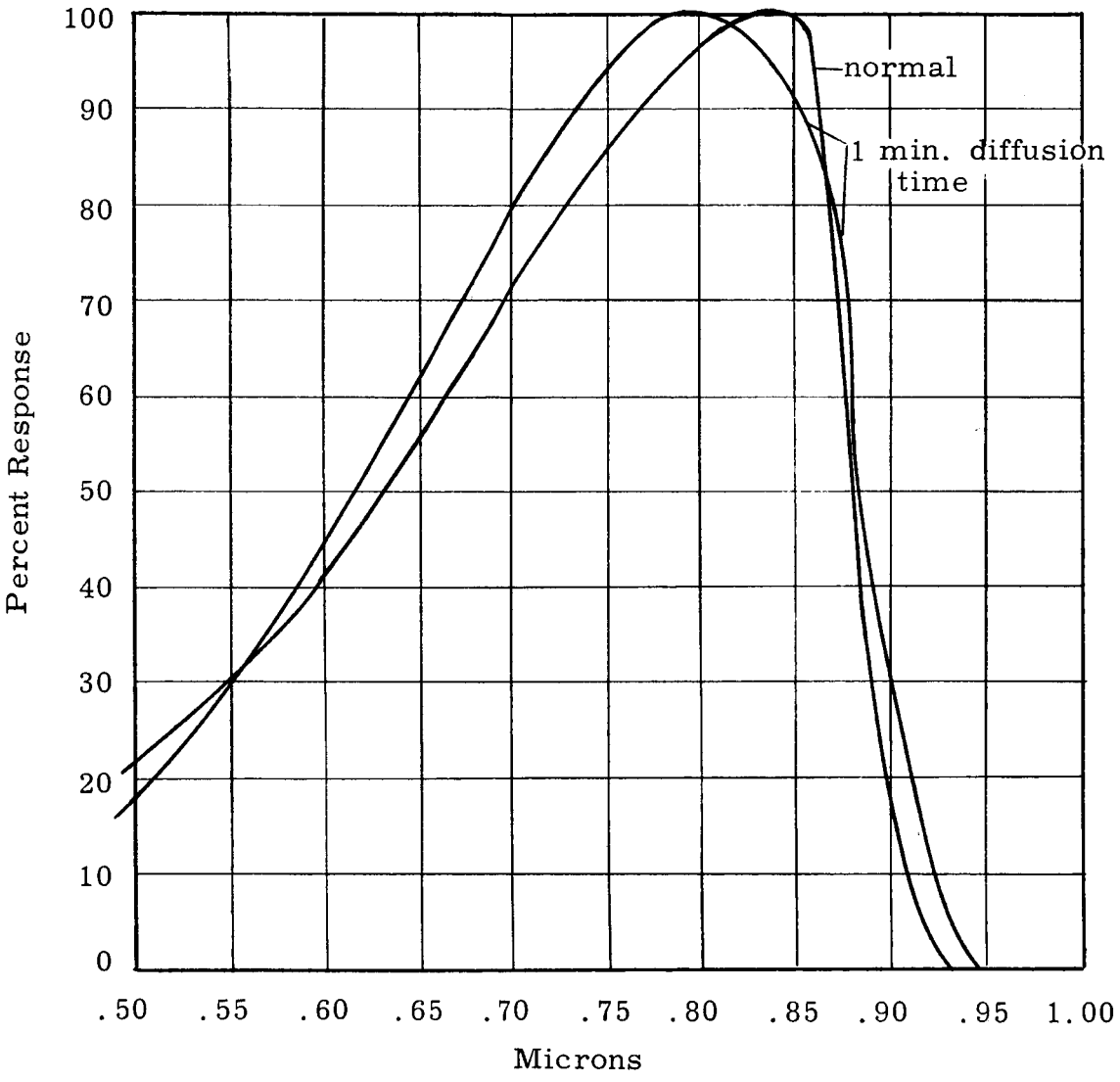

Fig. 2. GaAs Solar Cell Relative Spectral Response Versus Wavelength for Different Diffusion Times

gations indicated that a non-ohmic contact was being made to the "N" side of the device. Sn-Ni-Ag was tried and found to be significantly better than the Ti-Ag as an "N" contact. It was later found that the Ni was unnecessary, and Sn-Ag was used. The Ti-Ag "P" contact and the Sn-Ag "N" contact provides a strong contact mechanism (further discussed in Section C-4) having a series resistance of less than 1 ohm.

Several groups of cells were processed in order to evaluate 5 grid line cells and 7 grid line cells. The 7 grid line cells proved to have squarer V-I characteristics than the 5 grid line cells. The curve factor

$$\frac{V_p I_p}{V_{oc} I_{sc}}$$

was increased from an average of 60 for the 5 grid cells to an average of 68 for the 7 grid cells. Nine grid lines produced no increase in the curve factor, hence it was decided to fabricate all cells with 7 grid lines.

3. Optimization Etching

The optimization etch, as described in the section entitled Manufacturing Process, is a necessary compromise between diffusing deep enough to prevent shorting due to contact penetration and providing a junction extremely close to the surface. Data were taken on cells during the etching procedure to determine the relationship between conversion efficiency, sheet resistance and spectral response. Figure 3 shows the V-I characteristics with corresponding sheet resistance for a typical cell at each etch-time interval. Curve A was taken before any etching took place. Curve B was taken after a given time interval of etching. Curve C was taken after a second time interval and curve D after a third interval. Figure 4 shows the relative spectral response versus wavelength for the same cell with the A, B, C, D curves corresponding to the A, B, C, D curves of Fig. 3. As expected, the sheet resistance increases drastically and the spectral response curve is broadened as the surface is moved closer to the junction.

4. Soldering

The approach taken in developing a soldering mechanism was not to solder dip, or completely cover, the contact area but rather to spot solder connectors, or tabs, to the device. This approach is in keeping with the presently accepted method of attaching Si cells to solar panels.

Etch Step Sheet Resistance

A - 37 Ω/□
B - 58 Ω/□
C - 90 Ω/□
D - 145 Ω/□

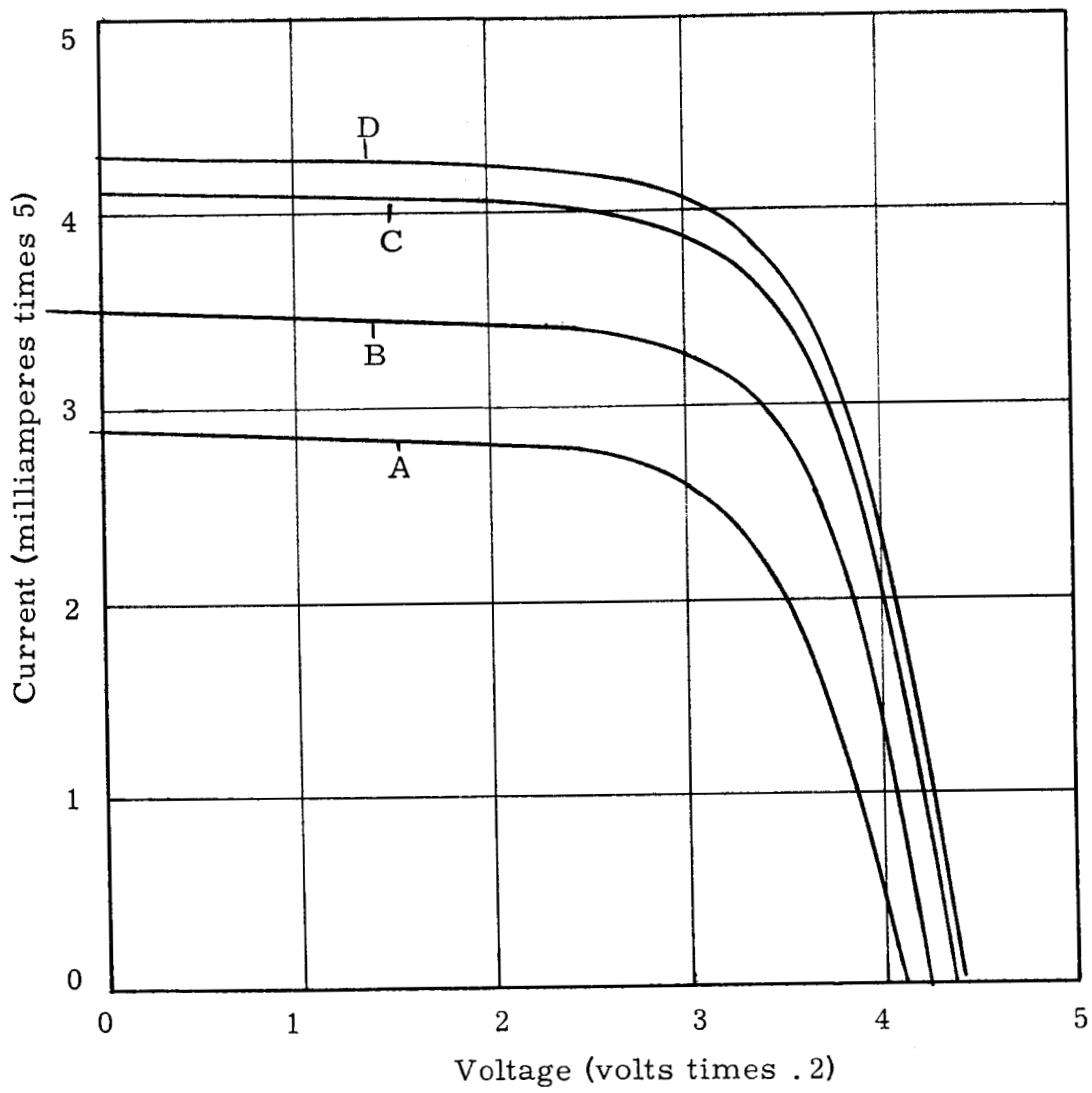

Fig. 3. V-I Characteristics During Optimization Etch Step With Corresponding Sheet Resistances

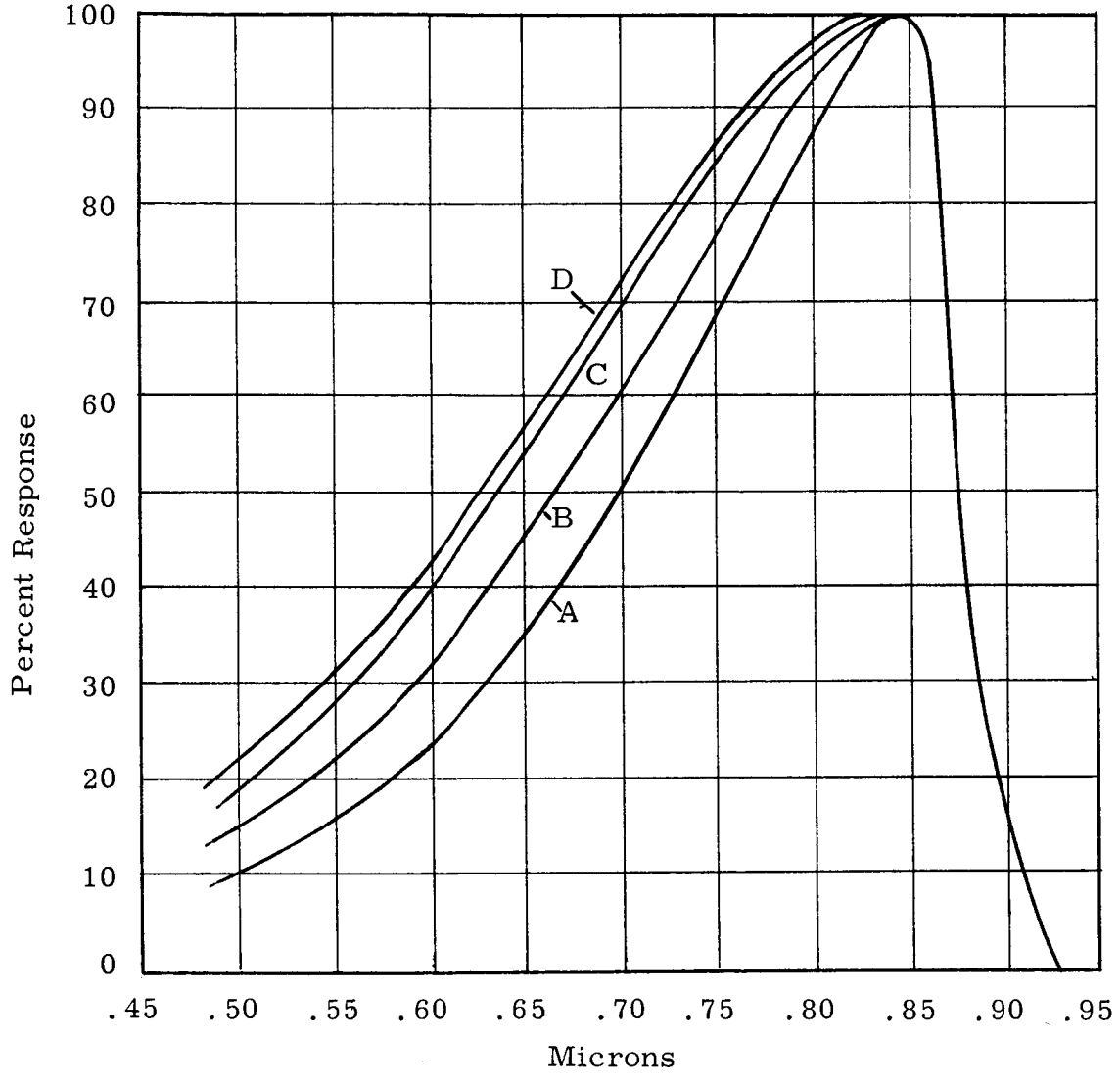

Fig. 4. GaAs Solar Cell Relative Spectral Response Vs. Wavelength With Curves Corresponding to Those of Fig. 1

The first attempts at soldering wires to the cells were less than satisfactory; however, with some minor changes, very good results were obtained.

First attempts involved Sn-Pb eutectic solder (melting point 183°C). If the soldering iron was allowed to remain in contact with the cell for any more than a brief period of time (approx. 3 seconds) there would be up to a 50% degradation in open circuit voltage. This degradation would occur only when solder was applied to the positive contact with no observable difference whether or not a wire was soldered or the positive contact just tinned. Soldering the "N" side did not affect the cell performance. By judicious use of the soldering iron, the problem was reduced but not eliminated.

It seemed obvious that thermal shock was causing the degradation. The cell was placed on a hot plate at a temperature just below the melting point of the solder. Solder and wires were applied to the cell while it was on the hot plate to reduce thermal shock. The results were very encouraging, therefore, the solder was changed from the lower melting point Sn-Pb to a In-Ag-Pb (2%-1.5%-96.5%) solder with a melting point of 305°C. Extremely good results were achieved by keeping the cell at approximately 260°C while soldering. Of 20 cells soldered, using the above method, there was no degradation observed in any of the cells.

The peel strength of the "N" contact has been in excess of 800 grams in all tests made. There was some question as to the mechanical reliability of the contact at elevated temperatures. A test was made to answer this question. Using the In-Ag-Pb material a wire was soldered to a cell. The cell was then placed on a hot plate and an 800 gram weight used to hold the cell in place. A pulling force estimated to be 300 to 400 grams was applied to the wire in an upwards direction normal to the cell. The hot plate was then turned on and an account was kept of the temperature. When the temperature reached 300°C the test was discontinued with no observable deterioration of the contact strength.

Peel strength of the "P" contact has been in excess of 300 grams and very little peeling has been observed. In most cases the cause of failure is attributed to the crystal fracturing under the contact. The actual peel failures appear to be of the same nature as peeled Si solar cells (the separation occurring at the Ti and Ag interface).

D. Measurements with Respect to Contacts, Material & Temperature Contacts

1. R-C and I_{sc}-V_{oc} Correlation, Ni:Ag Contracts

From a group of 40 cells, those representative of three widely separated performance categories were measured for series and shunt resistance, and capacitance. The groups, in terms of short-circuit current and open-circuit voltage were: (1) low current and low voltage, (2) low current and high voltage, (3) high current and medium high voltage. (Note: The combination high current and high voltage did not occur in this particular group of 40 cells.) The groupings of cells and corresponding R-C measurements are indicated in Table III. It is evident that no definite correlation existed between the R-C parameters and the current-voltage characteristics.

To further determine what specific basic differences separate the cells into the particular groups, the spectral response half-peak band widths were measured. The results, listed in Table IV show that the high current medium high voltage cells (group 3) exhibit a 25 to 50% broader spectral response than the low current cells (groups 1 and 2). This further verifies that the series and shunt resistances do not, in this case, uniquely determine the cell performance.

2. R-C and Efficiency Correlation Analysis, Sn:Ag Contacts

The use of Sn:Ag contacts lowered the 2 to 3 ohm series resistance measured for Ni:Ag contacts to about 0.1 ohms. Measurement of the basic resistance and capacitance characteristics of 23 cells from lots 66 through 69 showed the processing to have improved to a point where the effects of shunt resistance variations affect the cell efficiencies. The R-C and I_{sc}, V_{oc}, and η data is given in Table V. The basic parameter showing the most definite correlation with efficiency is the shunt resistance. This is indicated in Fig. 5. Capacitance values are also given for each resistance-efficiency point plotted.

3. Resistivity of Base Material

It was previously established on Contract NAS5-457, that the period of induced oscillations in the reverse biased cycle of a sinusoidal driven silicon solar cell varies inversely with the base resistivity as shown in the solid line experimental portion of Fig. 6 (see Appendix A). Assuming that the same empirical data can be extrapolated as shown and applied to the case of gallium arsenide solar cells, the resistivity of the processed gallium arsenide can be estimated and compared to data on the original crystal. The extrapolated portion

TABLE III

Resistance-Capacitance and Current-Voltage Distributions for Gallium Arsenide Cells Having Nickel:Silver Contacts

	V_{oc} (volts)							
	.760	.780	.800	.820	.840	.860	.880	.900
I_{sc} (ma)	.780	.800	.820	.840	.860	.880	.900	.920

49-50	C(uFd)	R_p(Ω)	R_s (Ω)
	0.082	420	2.5
50-51	0.086	1450	1.8
	Group I		
51-52			

C	R_p	R_s
0.077	460	2.1
0.081	380	2.1
0.089	9000	2.6
0.065	2000	3.1
0.066	230	2.1
0.060	630	1.7
0.055	320	1.7
Group II		

52-53

53-54

54-55

55-56

C	R_p	R_s
0.068	220	2.1
0.078	410	3.0
0.081	140	1.0
Group III		

56-57

57-58

58-59

TABLE IV

Spectral Half-Peak Band Width Correlation With Cell Performance

Category	Spectral Half-Peak Bandwidth, Microns	No. of Cells
1	.22 to .23	2
2	.20 to .24	3
3	.30 to .32	3

TABLE V

Resistance-Capacitance and Performance Characteristics for Tin:Silver Gallium Arsenide Cells Having Tin:Silver Contact Cells

Cell No.	Lot No.	C uFd	R_S ohms	R_p ohms	I_{sc} ma	Voc volts	η * %
1	66	0.0722	0.40	140	20.4	.900	6.8
2	66	0.0772	0.40	670	18.9	.890	7.0
3	66	0.0718	0.40	320	19.9	.896	8.0
4	66	0.0673	< 0.30	100	22.0	.910	8.8
5	66	0.0724	< 0.30	120	21.0	.890	7.0
6	66	0.0569	< 0.30	850	25.5	.938	10.5
1	67	0.0483	< 0.30	370	20.7	.850	7.5
2	67	0.0517	< 0.30	680	22.5	.880	8.4
3	67	0.0550	< 0.30	240	22.5	.820	6.8
4	67	0.0522	< 0.30	4700	23.0	.900	9.0
5	67	0.0529	< 0.30	500	23.9	.890	9.0
6	67	0.0491	0.40	200	19.9	.804	< 6.5
1	68	0.0571	0.40	1600	24.0	.894	9.0
2	68	0.0570	< 0.30	380	23.4	.880	8.5
3	68	0.0544	< 0.30	1100	23.9	.900	9.4
4	68	0.0566	< 0.30	150	23.0	.884	7.5
5	68	0.0570	< 0.30	400	22.5	.872	8.0
1	69	0.0532	0.40	4200	23.8	.880	9.0
2	69	0.0511	< 0.30	900	22.8	.868	8.5
3	69	0.0500	< 0.30	800	24.6	.910	9.5
4	69	0.0590	< 0.30	4000	21.2	.890	8.3
5	69	0.0550	< 0.30	900	24.0	.886	9.5
6	69	0.0522	0.40	8200	21.7	.884	8.5

C = junction capacitance at V = O
R_S = series resistance
R_p = shunt resistance
I_{sc} = short circuit current
V_{oc} = open circuit voltage
η = efficiency

*efficiency under 2800°C tungsten source, 100 milliwatt/cm^2 equivalent

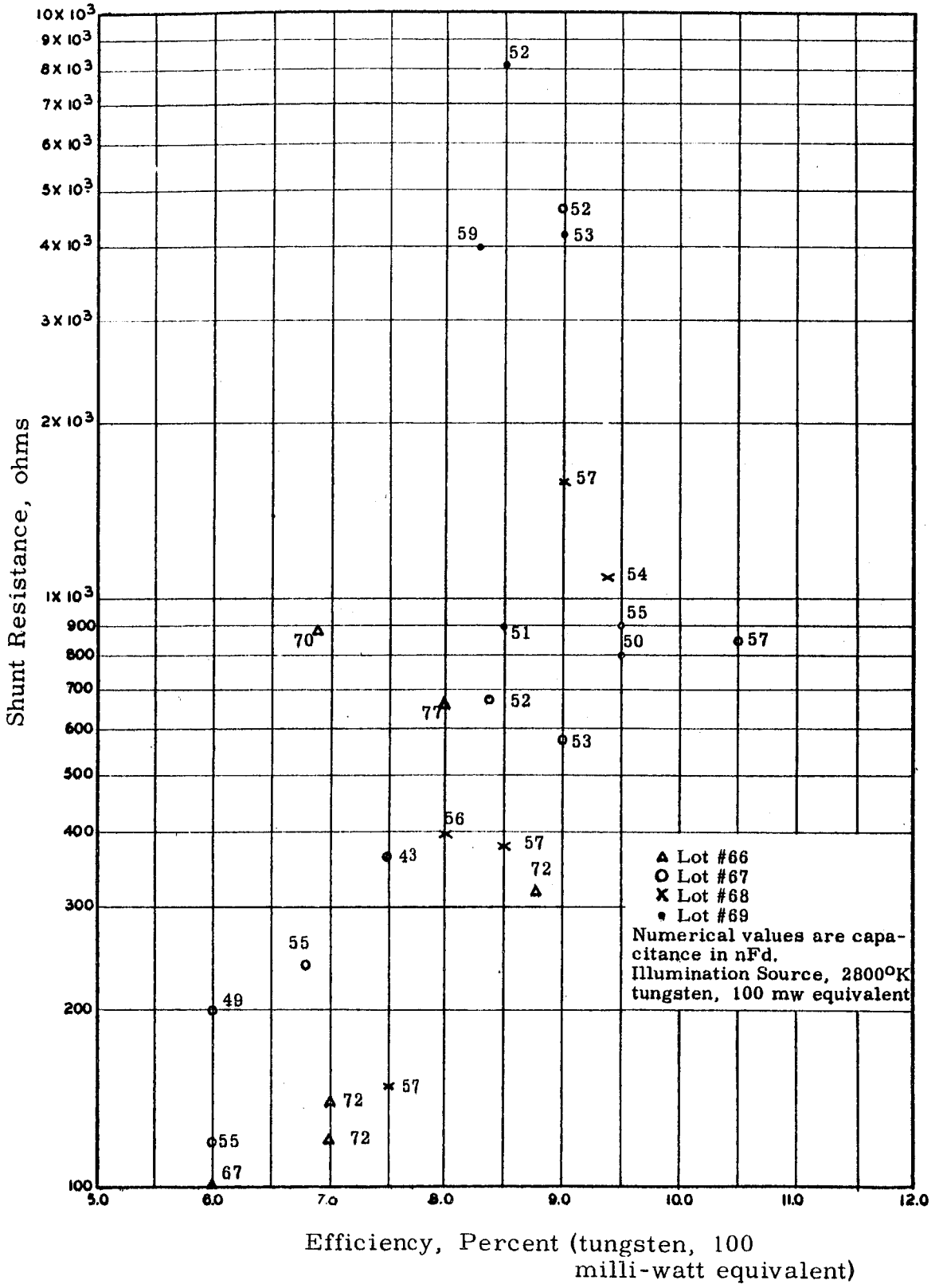

Fig. 5. Cell Efficiency Correlation with Shunt Resistance

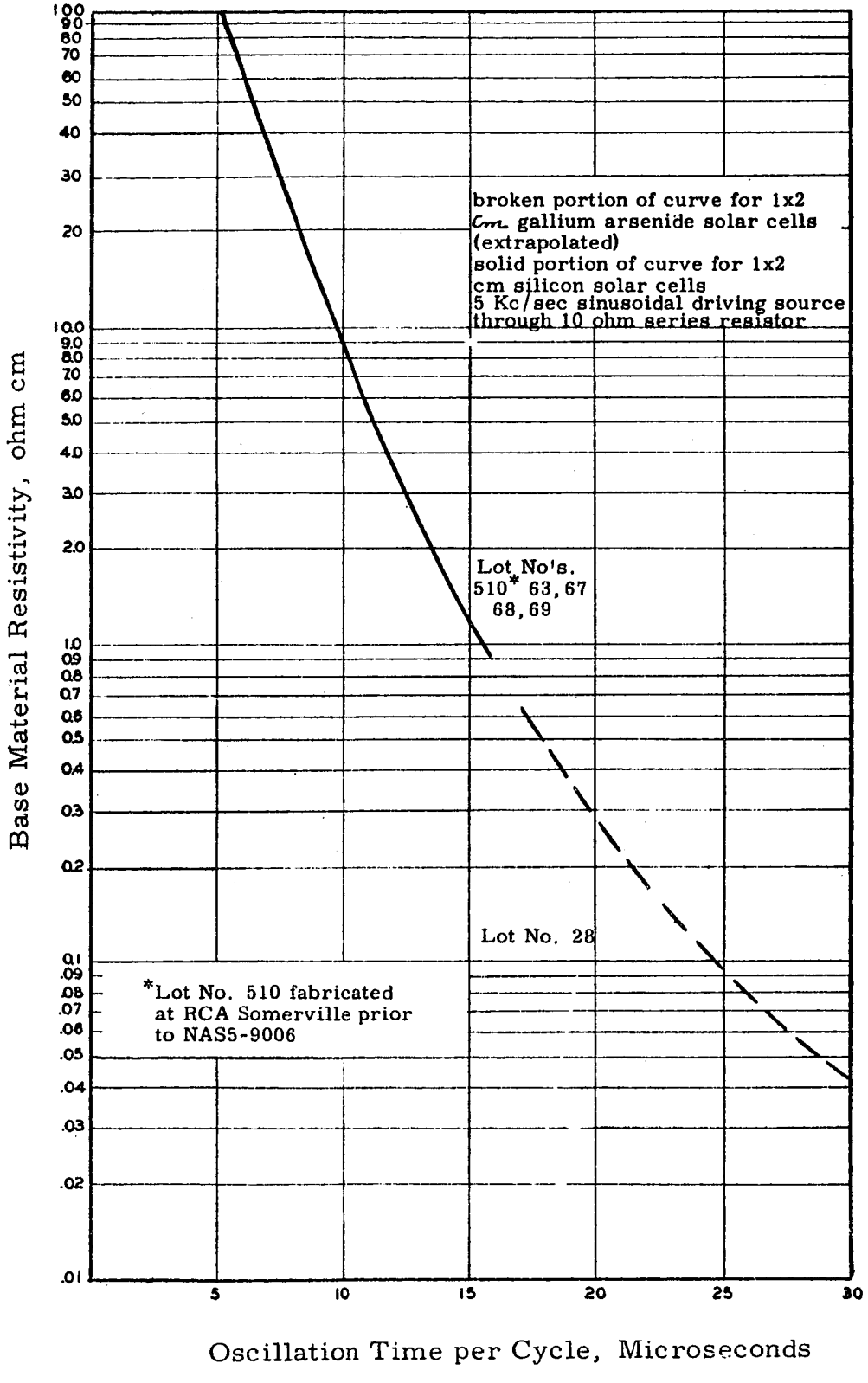

Fig. 6. Oscillation Period of Reverse Bias Transient Versus Base Resistivity

of Fig. 6 covers a greater range than the 0.02 to 0.1 ohm cm reported for the starting material. The empirical data suggests the range to extend from 0.04 to 0.5 ohm cm. The discrepancy is not excessive. Comparison of the cell efficiencies for the various lots processed has not shown any significant correlation with the base resistivity as noted from the listing given in Table VI.

4. Mass Spectrographic Analysis of Gallium Arsenide

The MS-7 mass spectrograph has been used for the analysis of 12 n-type germanium doped gallium arsenide sample from 6 separate ingots. Twenty impurity elements were detected, three (namely Si, Ge, and S) are n-type dopants. C, O, Mg, Fe, Si, and Al were present in more than 50% of the samples in concentrations greater than 0.1 part per million. Although Te was reported by the vendor to be the dopant for one ingot (two samples), its presence, was not detected even though the detection limit for this element is 0.4 parts per million. The range of concentrations of the major impurities is indicated in Table VII. Significantly, the arsenic concentration was 1 to 122% of the gallium concentration.

If an experimental error of a factor of 3 is assumed for the mass spectrograph then 6 of the 12 samples could not be stoichiometric. From the large variation it seems that the possibility of non-stoichiometry is realistic. It is interesting to note that the amount of Si and Al impurities increase as the As to Ga ratio gets smaller. This is demonstrated in Table VIII. It should also be noted that in most cases the As to Ga ratio was relatively consistent in a given crystal. No definite corrolation could be made between the cell performance and the As to Ga ratio, however, this could be due to process changes. Due to the large variation and apparent symmetry of the data obtained from the mass spectrograph it is suggested that this area be investigated in future work done on the device.

5. Optical Characteristics

a. Reflectance of GaAs - Figure 7 gives the measured reflectance of a GaAs solar cell with and without the silicon monoxide anti-reflective coating. For comparison purposes, the relative transmission curve through 16 mils of GaAs and the relative spectral Response curve of a GaAs solar cell are also included. (Both of these curves are normalized to a numerical value of 30 for convenience.)

The effectiveness of the SiO anti-reflective coating is apparent. Incomplete reduction of reflectance in the region between 0.74

TABLE VI

Measured Oscillation Period of Reverse Bias Transient and Efficiencies of Gallium Arsenide Solar Cells

Lot	Oscillation Period Max. usec	Oscillation Period Min. usec	Number of Cells Sampled	η Efficiency Max. Percent	η Efficiency Min. Percent
510*	22	18	10	10.0	6.1
8	26	-	1	7.3	-
11	25	-	1	9.2	-
14	26	-	1	9.6	-
16	26	25	3	9.1	7.4
17	30	27	4	9.2	7.7
18	28	26	6	9.0	7.6
19	27	26	6	10.1	8.9
20	31	28	2	8.7	8.0
21	28	-	2	8.9	8.7
24	28	27	2	8.8	7.7
28	30	24	5	11.1	9.0
29	25	24	5	9.9	8.2
66	24	22	7	10.5	6.5
67	21	19	6	9.0	6.5
68	21	19	5	10.5	6.5
69	20	18	7	9.5	8.3

*Lot 510, fabricated at RCA Somerville prior to NAS5-9006.

Table VII

Concentrations of Major Impurities
in Gallium Arsenide

Percentage of Samples in Concentration Range Concentration, Parts per Million (Gallium at 5 x 10^5 parts per million is the reference)									
Element	0 to 0.009	0.010 to 0.249	0.25 to 0.98	1.00 to 4.99	5 to 9.99	10 to 14.9	15 to 19.9	20 to 24.9	25 to 49.9
B	83	8		8					
F	50	50							
Mg		92		8					
Al		58		33					8
P	33	67							
Ca	92	8							
Cr	100								
Fe	67	25	8						
Cu	100								
Cl	*	25							
Si			25	33	25	8		8	
K	*	8							
In	50	50							
Ge	*			8	8				
Pb	*	8	8						
S	*		17						

Note 1: *Presence of element not detected except in concentration cited.

2: C & O were detected but are variables depending on the background at the time of analysis.

Table VIII

Correlation of Impurities to the Arsenic to Gallium Ratio

Crystal No.	Arsenic to Gallium Ratio	Concentration of Elements, Parts per Million												
		Si	Al	Mg	Fe	Cu	Ge	S	Pb	In	Ca	P	O	Cl
861	.01	22	2.3	.12		.1						.1	1.4	
887	.05	12	1.7	.13		.1						.2	.4	
861	.08	9.7	46*	4.5	.3					.2	.1		35	
A	.18	1.1*	1.1	.1	.2				.2				.5	
916	.20	5.0	.1	.2	.1								.5	.1
A	.28	2.4*	4.8*		.2						.2		.8	.3
916	.36	6.0	.1	.1	.1	.1				.1			1.3	
887	.38	3.0	0.4*	.1	.2				.4	.2			1.1	
915	.40	1.2	.1	.1									.5	
915	.58	1.0	.1	.1									.3	
920	1.02	0.5*	.1	.2			2.6	.9					1.5	
920	1.22	0.9	.1	.2	.1		6.4						.9	

Note 1: Gallium at 5×10^5 parts per million is taken as the reference.

2: *Samples which do not fit the correlation with respect to the arsenic gallium ratio.

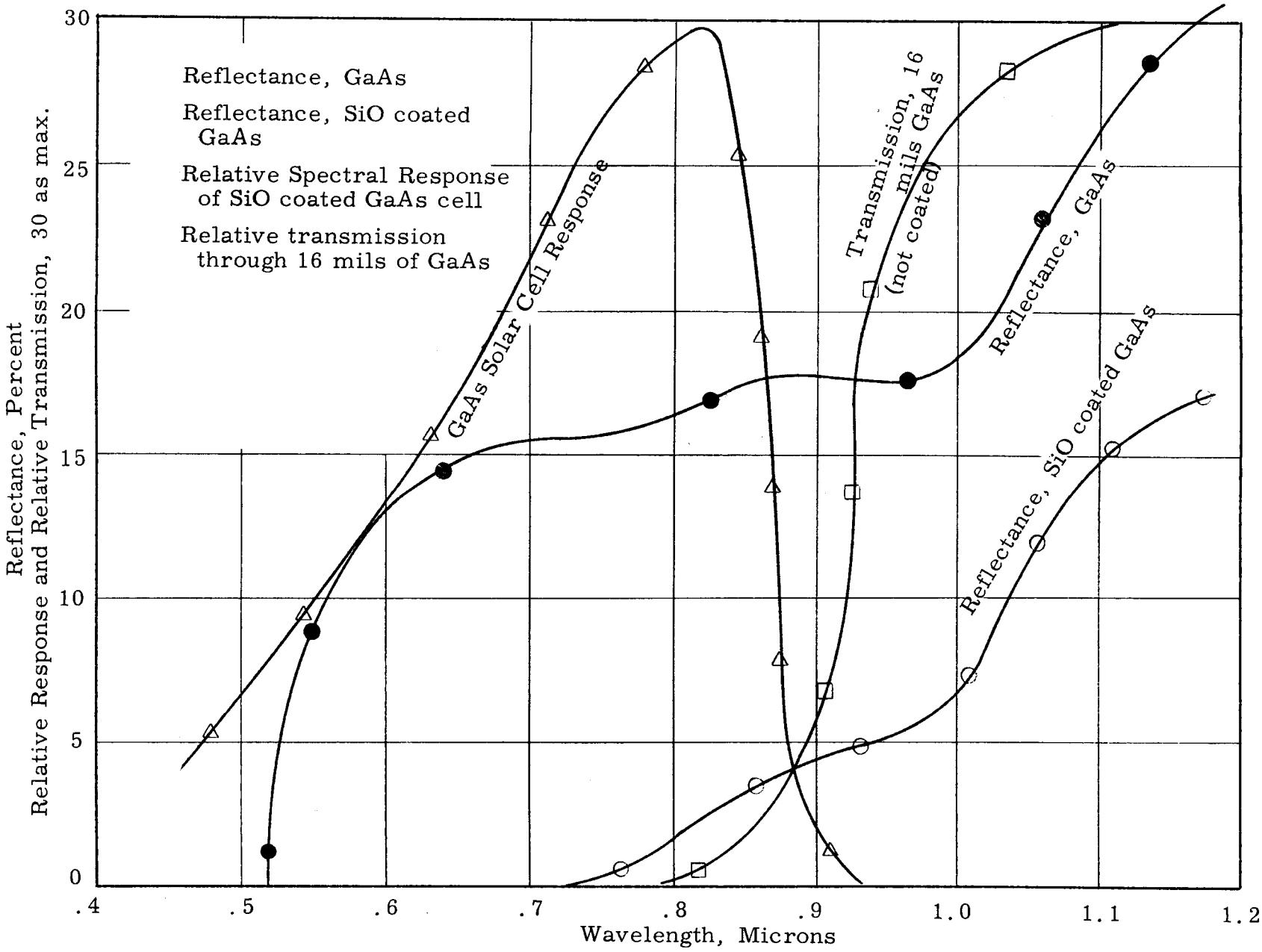

Fig. 7. Reflectance Characteristics of GaAs and Silicon Monoxide Coated GaAs

and 0.93 microns may result from reflection from the Sn:Ag grids, or further optimization of the SiO coating may be required.

It is to be noted that no marked change in reflectance for the GaAs (no coating) occurs in the spectral region of the optical transmission cut-off at 0.8 microns for GaAs. Therefore, the optical transmission curve as presented does not have any appreciable reflectance properties superimposed. This is particularly relevant to the conclusions of Section b below regarding transmission through zinc diffused GaAs relative to undiffused GaAs.

b. Optical Transmission Through GaAs and Zinc Diffused GaAs - Figures 8 and 9 give the optical transmission curves of GaAs and Zinc diffused GaAs. The curves were taken at constant slit width on the spectrophotometer and are therefore nearly constant bandwidth curves for the spectral region considered. The curves of Fig. 8 were taken with the polished face of the GaAs facing the illumination source; the curves of Fig. 9 are for the non-chem-polished back surface facing the source. Although these curves have the GaAs absorption characteristic superimposed on the tungsten source spectrum, it is apparent that the zinc diffused cells show about a three percent loss in optical transmission compared to non-diffused GaAs in the 0.87 micron region, i.e., near the optical absorption edge of GaAs. These preliminary results indicated further analysis of the effects of zinc diffusion on optical transmission is warranted.

6. Temperature Vs. Cell Parameters Measurements

Figure 10 represents V-I curves at various temperatures of a typical GaAs solar cell. Figures 11 through 17 represent typical values for the cell parameters vs. temperature. Typical Si solar cell curves are presented for comparison. The curves of Fig. 10 were made using 100 mw/cm^2 of tungsten light at a color temperature of 2800^{o}K.

7. Spectral Response Vs. Temperature

Spectral response data were recorded as a function of temperature using a Perkin-Elmer spectrophotometer with a temperature-controlled cell holding fixture. Data were taken at cell temperatures of 28^{o}C, 50^{o}C, 100^{o}C, 150^{o}C, 200^{o}C and 250^{o}C. There is a shift in the response toward the long wavelength region as the temperature

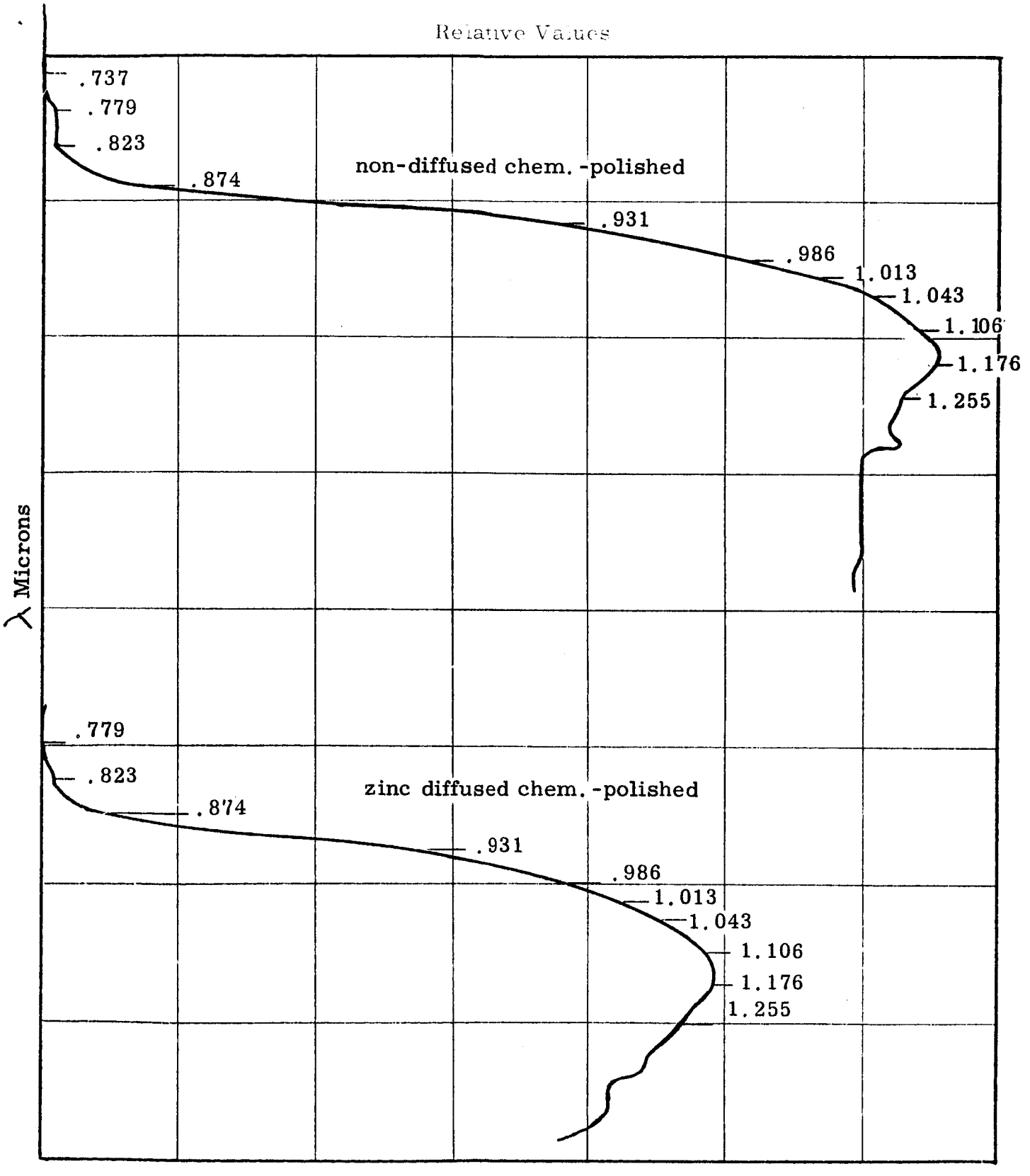

Fig. 8. Optical Transmission Curves of GaAs and Zinc Diffused GaAs

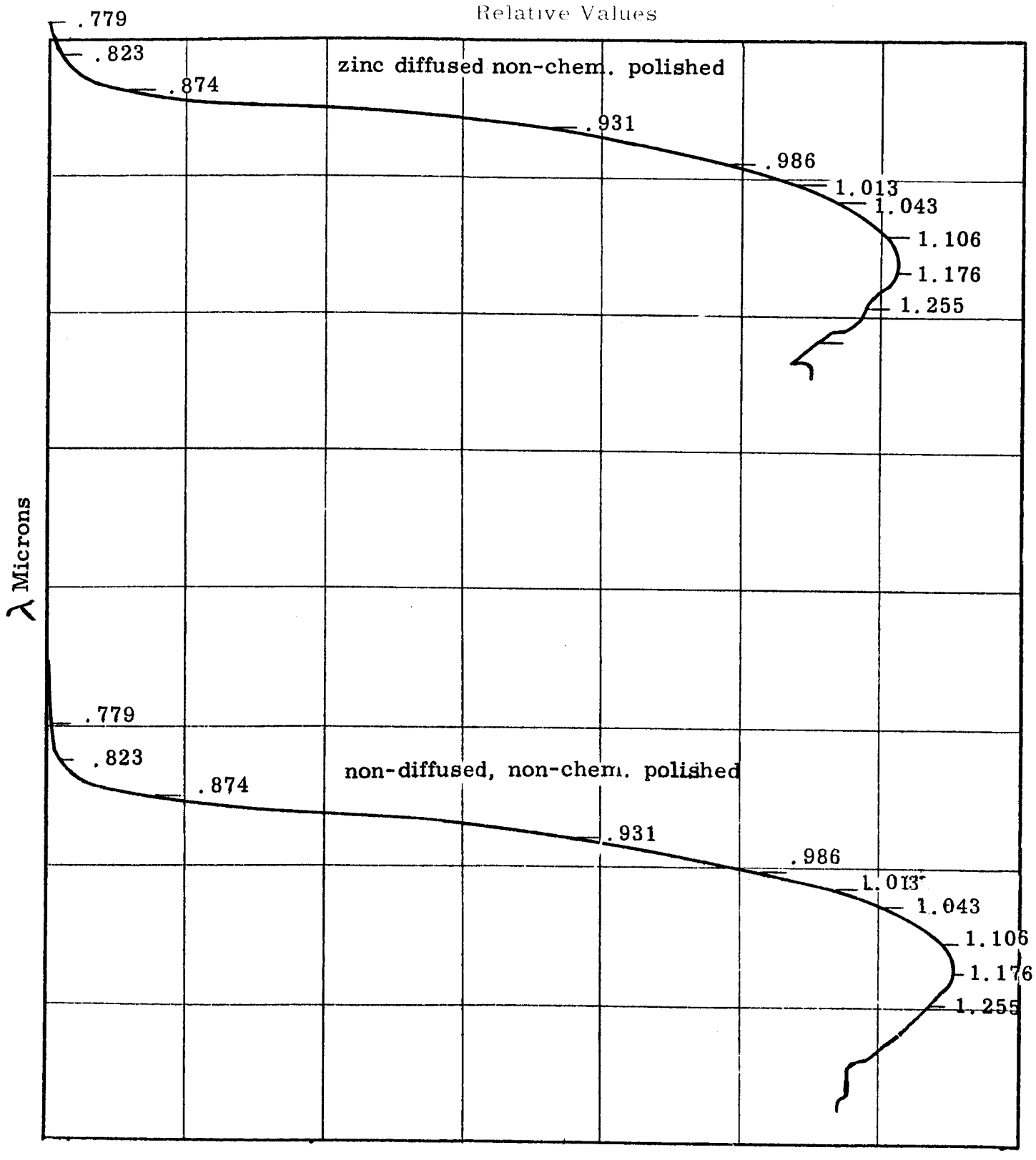

Fig. 9. Optical Transmission Curves of GaAs and Zinc Diffused GaAs

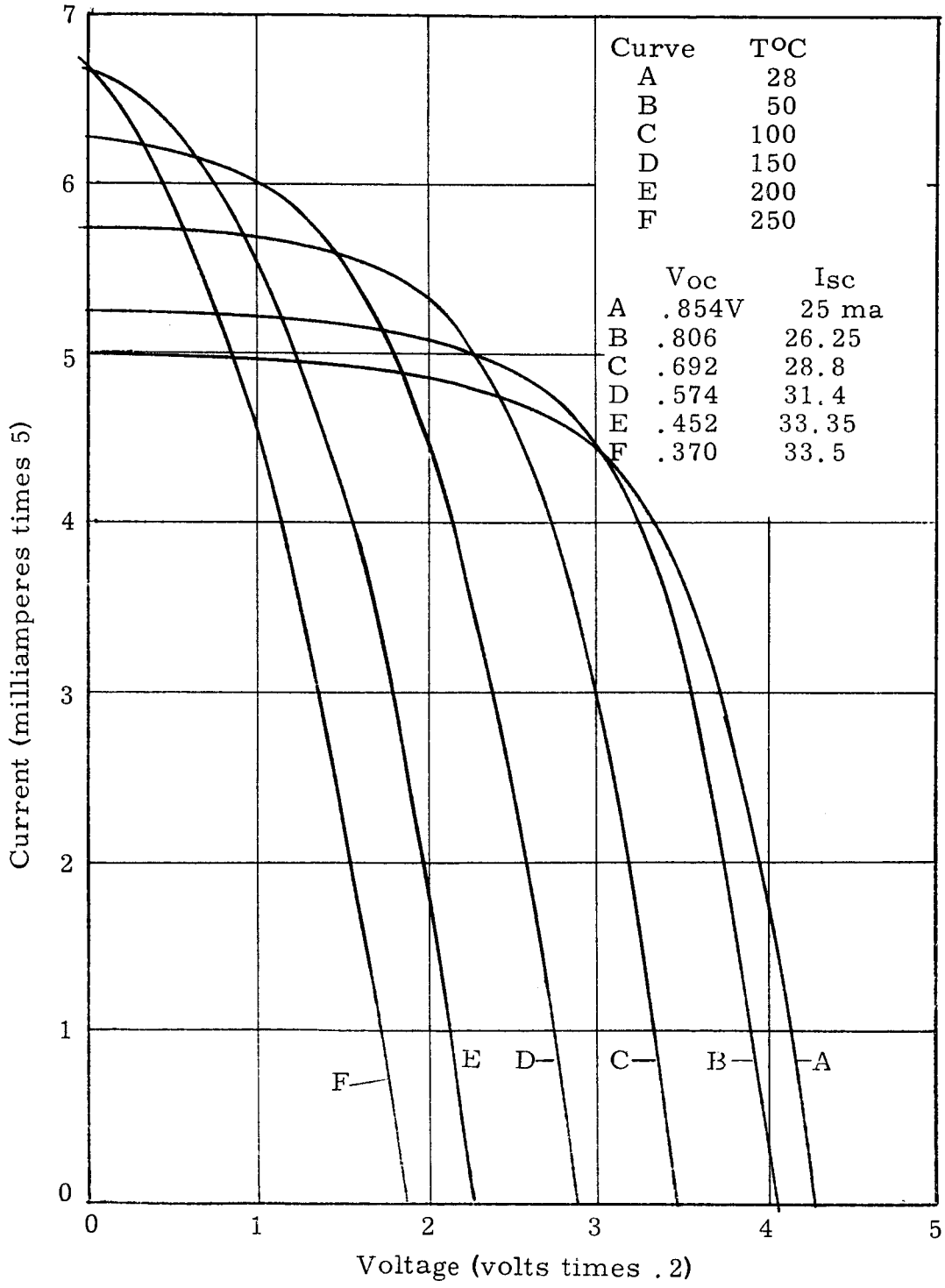

Fig. 10. Current Voltage Characteristics Versus Temperature

— V_{oc} $50^{\circ}C$ / $200^{\circ}C$ $\quad \frac{354 \text{ mv}}{150^{\circ}C} = -2.36 \text{ mv}/^{\circ}C$

– – – V_{mp} $50^{\circ}C$ / $200^{\circ}C$ $\quad \frac{320 \text{ mv}}{150^{\circ}C} = -2\ 1 \text{ mv}/^{\circ}C$

— voltage at open circuit

– – – voltage at maximum power point

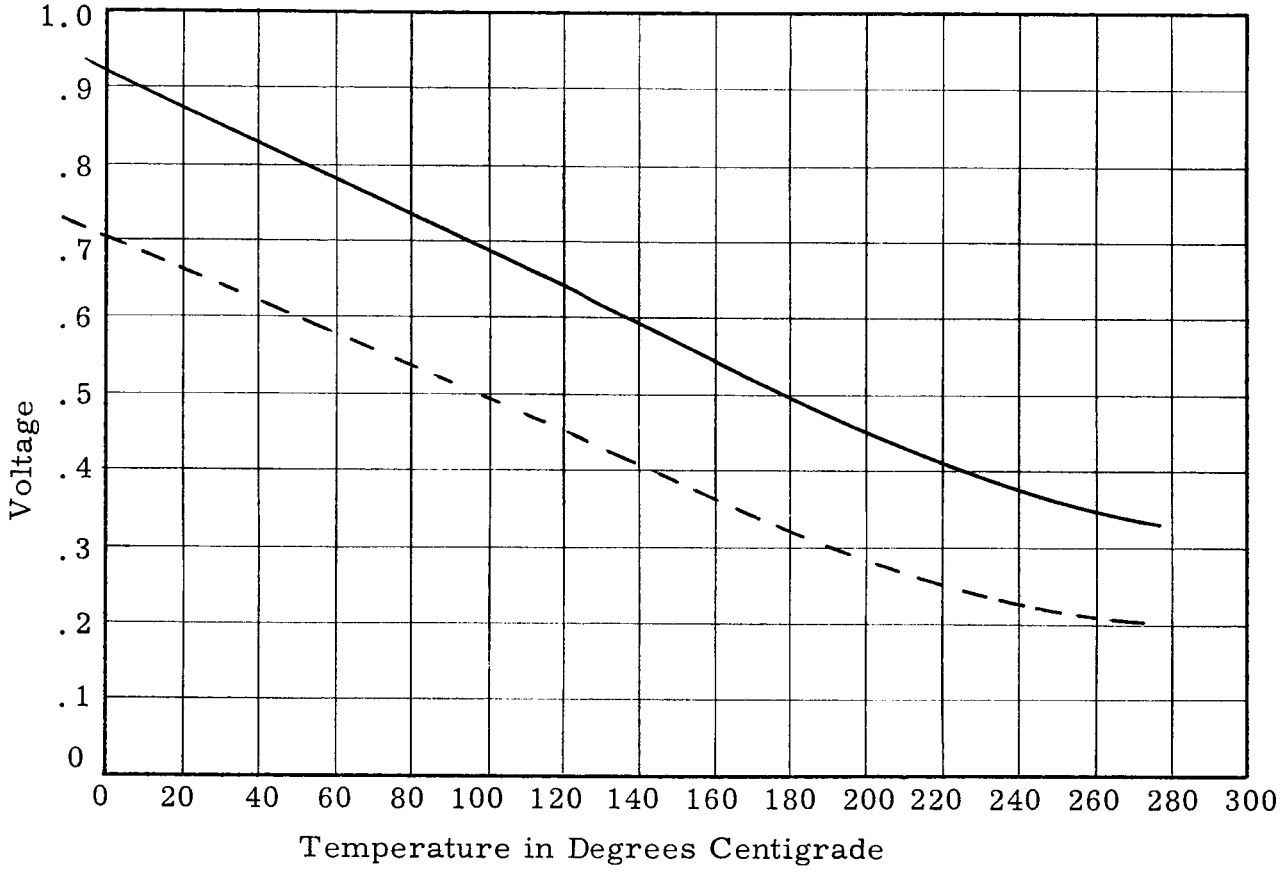

Fig. 11. Graph of Voltage Vs. Temperature for a Gallium Arsenide Solar Cell (1 x 2 cm P on N)

$$\text{——}\ V_{oc}\ \begin{matrix}50^{\circ}C\\200^{\circ}C\end{matrix} = \frac{352\ mv}{150^{\circ}C} = -2.35\ mv/^{\circ}C$$

$$\text{– – –}\ V_{mp}\ \begin{matrix}50^{\circ}C\\200^{\circ}C\end{matrix} = \frac{315}{150^{\circ}C} = -2.1\ mv/^{\circ}C$$

—— voltage open circuit

– – – voltage maximum power

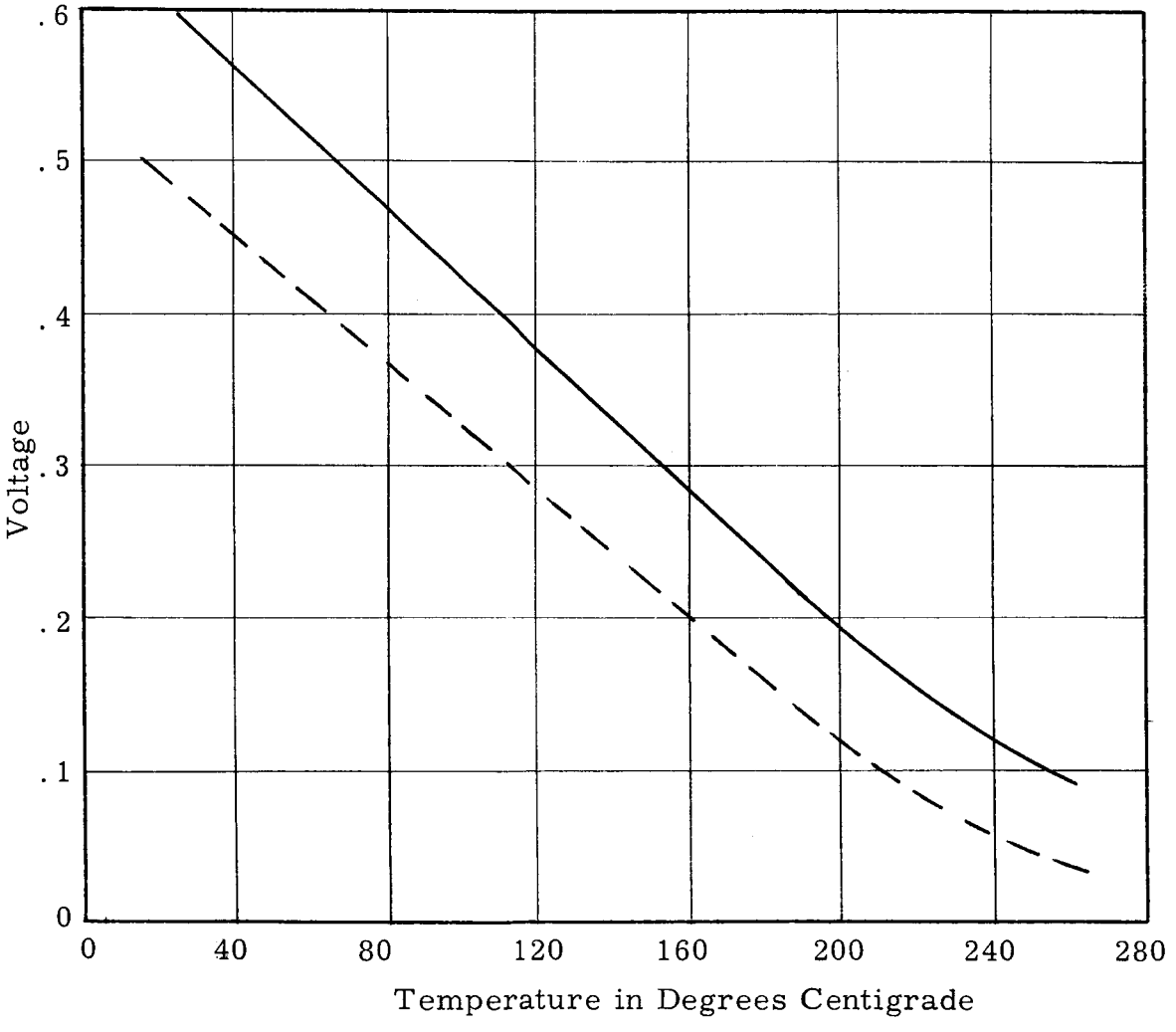

Fig. 12. Graph of Voltage Vs. Temperature for a 2 x 2 cm Silicon Solar Cell (N on P)

$$\text{—}I_{sc}\ \begin{matrix}50^{o}C\\200^{o}C\end{matrix}\ \frac{7100\ ua}{150^{o}C} = 47.3\ ua/^{o}C$$

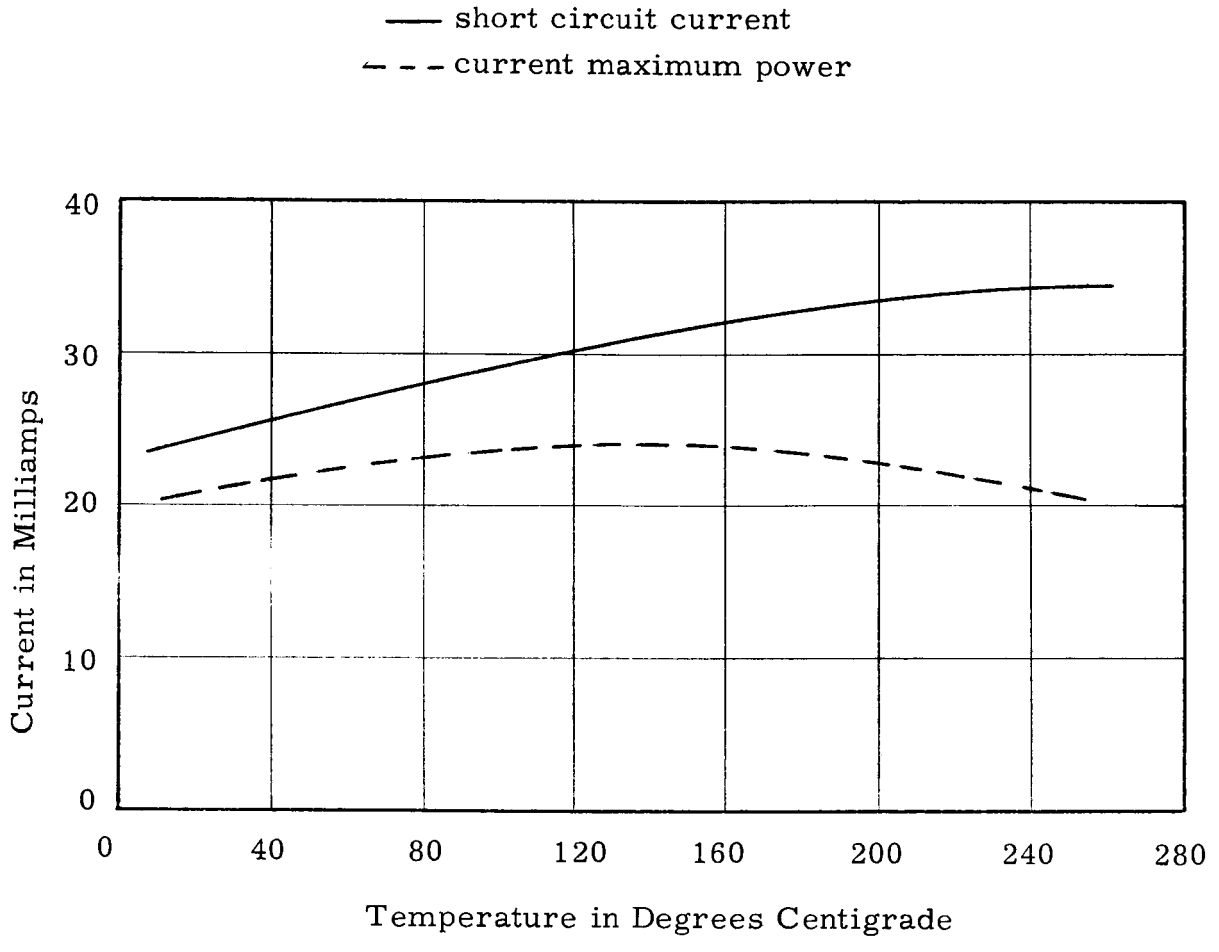

Fig. 13. Graph of Current Vs. Temperature for a Gallium Arsenide Solar Cell (1 x 2 cm P on N)

Power $\begin{matrix} 50^{o} \\ 200^{o} \end{matrix}$ $\frac{7.05 \text{ mw}}{150^{o}\text{C}} = -.047 \text{ mw}/^{o}\text{C}$

Eff. $\begin{matrix} 50^{o} \\ 200^{o} \end{matrix}$ $\frac{3.91}{150^{o}\text{C}} = -.026\%/^{o}\text{C}$

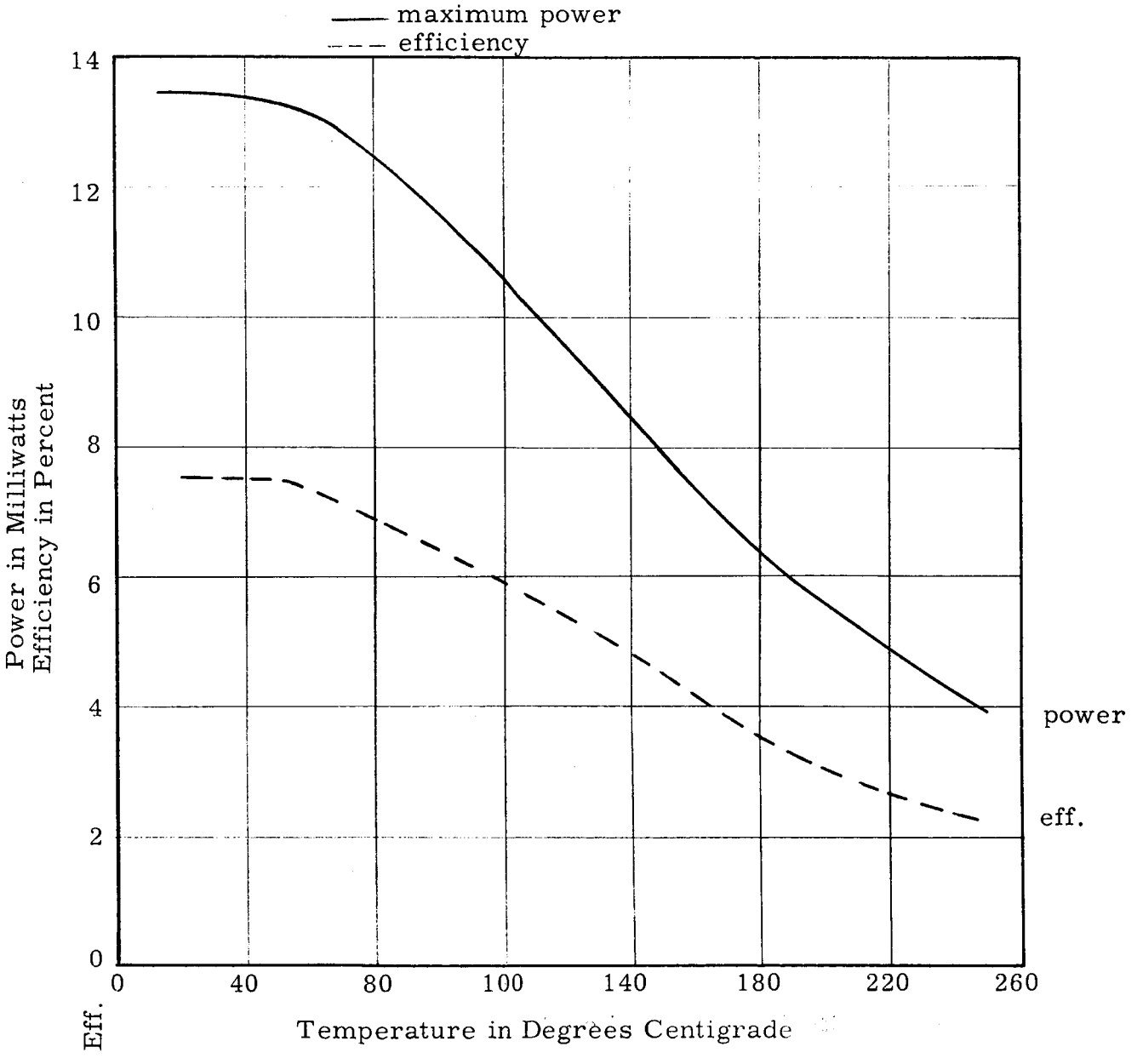

Fig. 14. Graph of Temperature Vs. Efficiency and Maximum Power of 1 x 2 cm Gallium Arsenide Solar Cell (P on N)

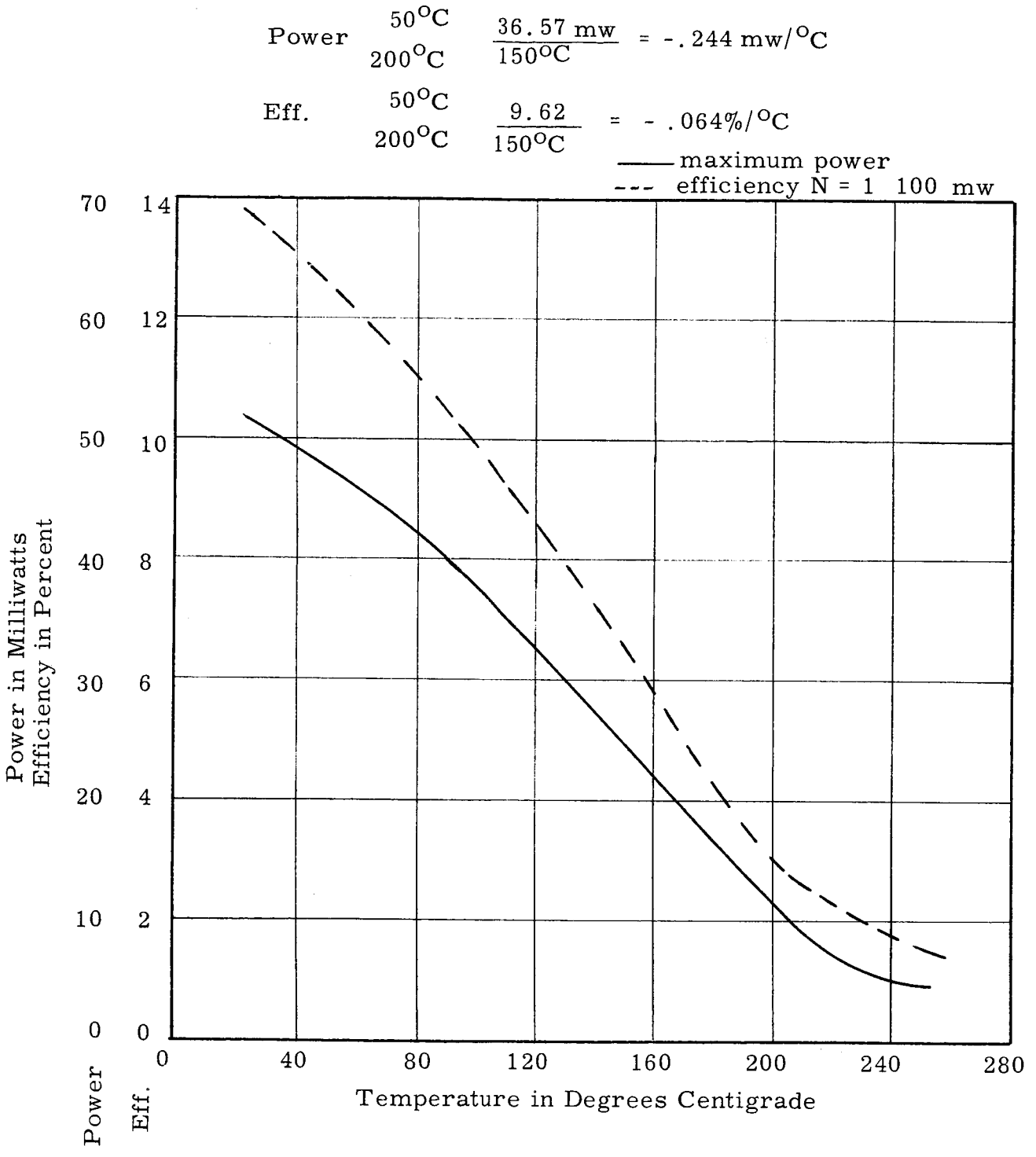

Fig. 15. Graph of Temperature Vs. Efficiency and Maximum Power of a 2 x 2 cm Silicon Solar Cell (N on P)

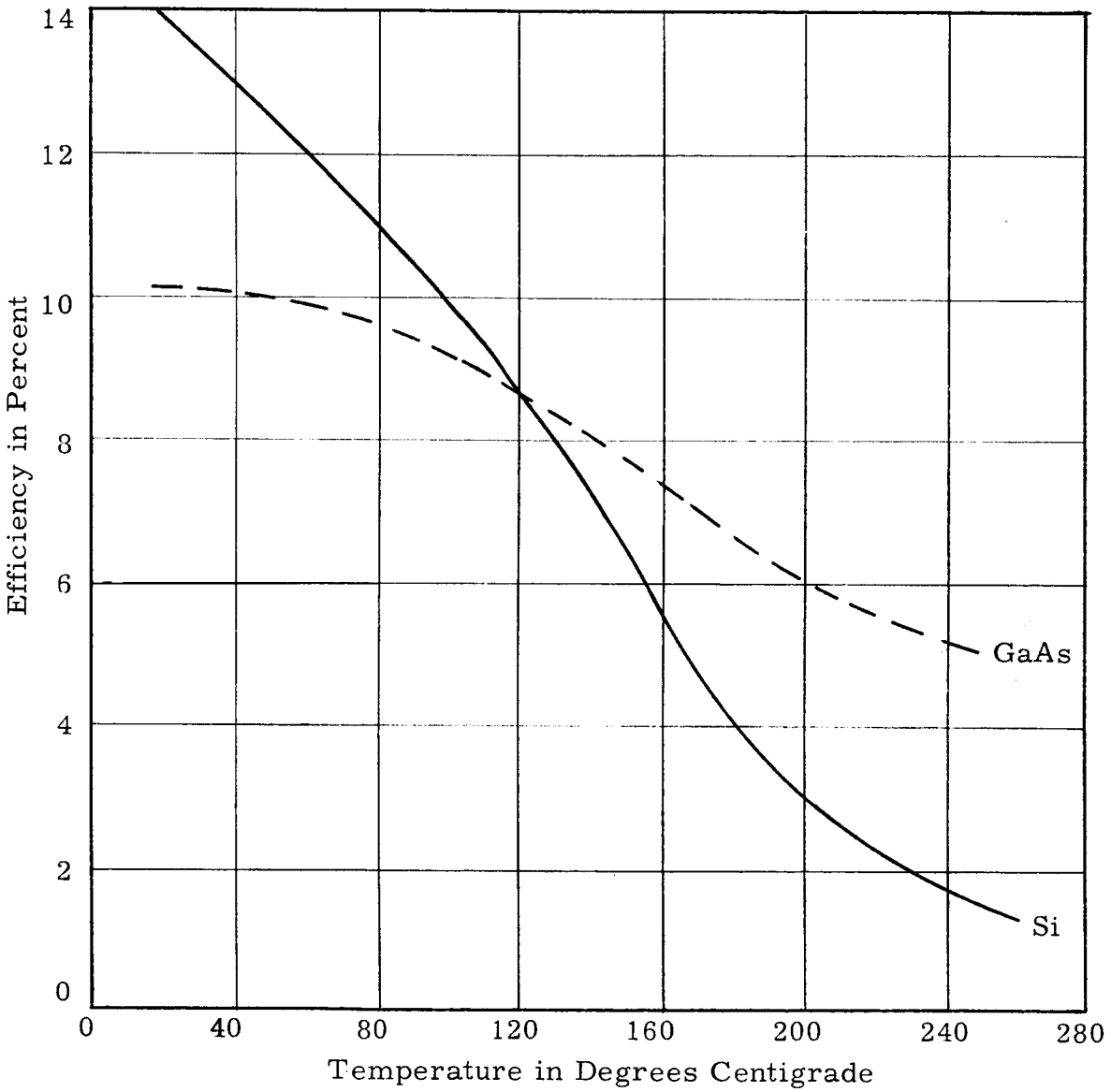

Fig. 16. Graph of Efficiency of GaAs and Si Solar Cells at Today's Potential Best Efficiency for Tungsten - 100 mw/cm^2

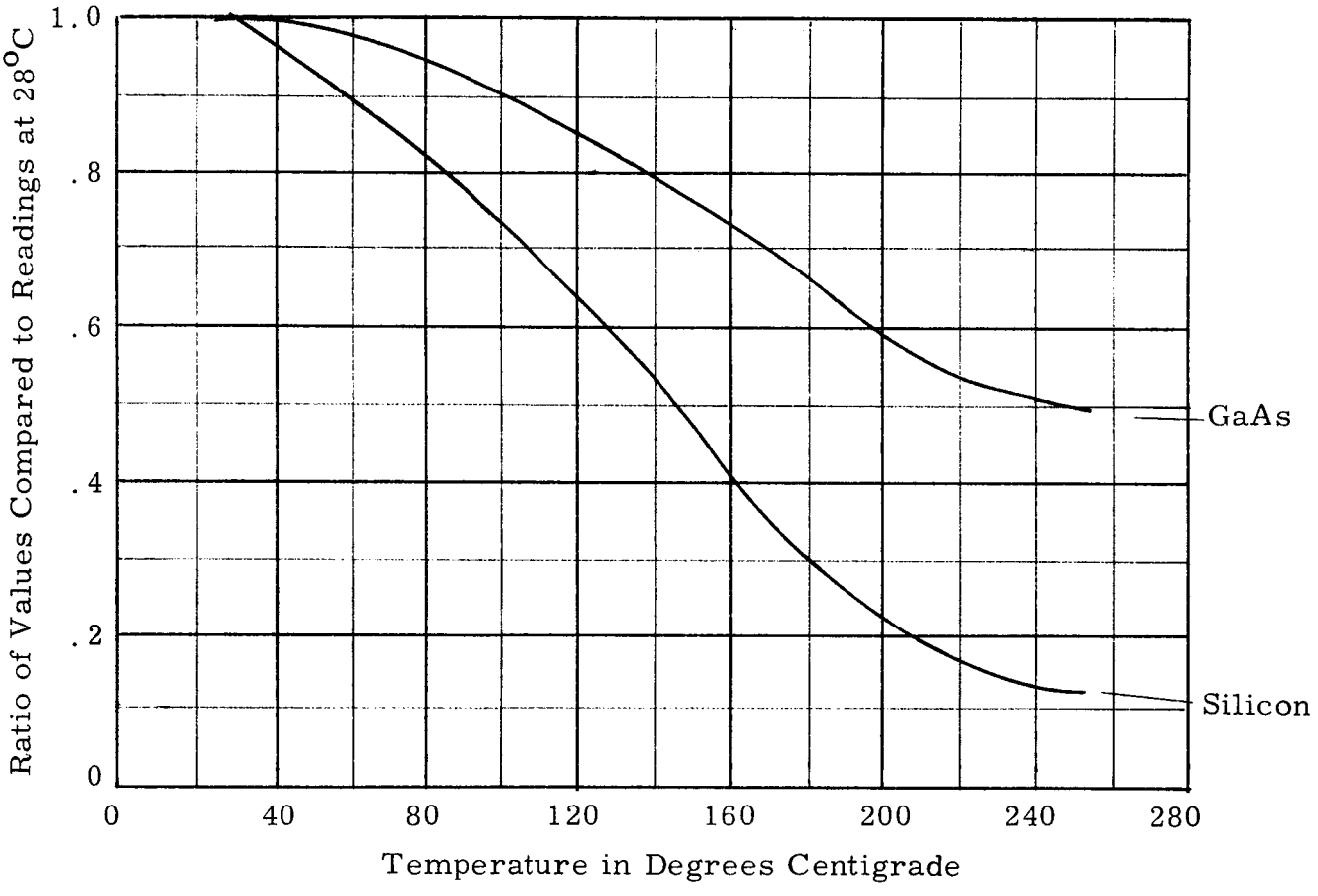

Fig. 17. Efficiency Ratio Versus Temperature

is increased. Figure 18 is a graph of the ratio of the normalized spectral response value at various temperatures to the normalized spectral response value at 28°C plotted against wavelength (0.50 microns to 0.825 microns). For example, at 0.50 microns there is 28% less response at 250°C than at 28°C, at 200°C there is 22% less response than at 28°C, etc. It should be mentioned that the results are not as drastic as they may appear in Fig. 18. When the device's normalized spectral response is combined with the solar spectral distribution (Johnson's data), there is very little change in the calculated resultant response of the cell at various temperatures due to the gain in red response compensating the loss in blue response. Unfortunately, a graphical display of this is not possible due to the sensitivity of the measuring equipment.

E. High Temperature Storage Testing

High temperature storage tests were performed at temperatures which presently define the upper operating limit of GaAs solar cells. Temperatures of 200°C and 250°C were chosen for initial tests.

The first group, fabricated with Ti-Ag contacts on both sides of the cell, was tested after 0, 25, 134, 350, and 950 hours of storage. Tables IX and X give the results of the 200°C test and the 250°C test respectively. Comparison of the parameters in both groups show approximately the same magnitude of change (except cell 18-4 in the 250°C group) as illustrated by the percent change. If the cause of the changes was thermally sensitive, it would be expected that the cells stored at 250°C would degrade more than those stored at 200°C. No explanation can be given for the catastrophic degradation of cell 18-4.

The second group, fabricated with Sn-Ag back and Ti-Ag front contacts, was tested after 0, 137 and 323 hours of storage. Tables XI and XII give the results of the 200°C test and 250°C test respectively. The average percent change for the 250°C test shows slightly higher degradation than the 200°C test; however, all data is in reasonable agreement with the results of the first group when measured at 139 and 350 hours. For comparison, Table XIII gives parameter changes for Si solar cells stored at 250°C.

The series and shunt resistances and junction capacitance data taken at 0, 137 and 323 hours are presented in Table XIV. It was concluded that the cause of degradation was not due to a physical change in the junction or to a failure in the contact structure, since the junction capacitance and series resistance showed no change. Several of the cells showed a degradation in the knee of the V-I curves. As can be seen in Table XIV, there is a decrease in the shunt resistance, R_p, in many of the cells.

$$R = \frac{\text{Normalized value @ T } (X^{o}C)}{\text{Normalized value @ T } (28^{o}C)}$$

$T(X^{o}C)$ = Temperature in question

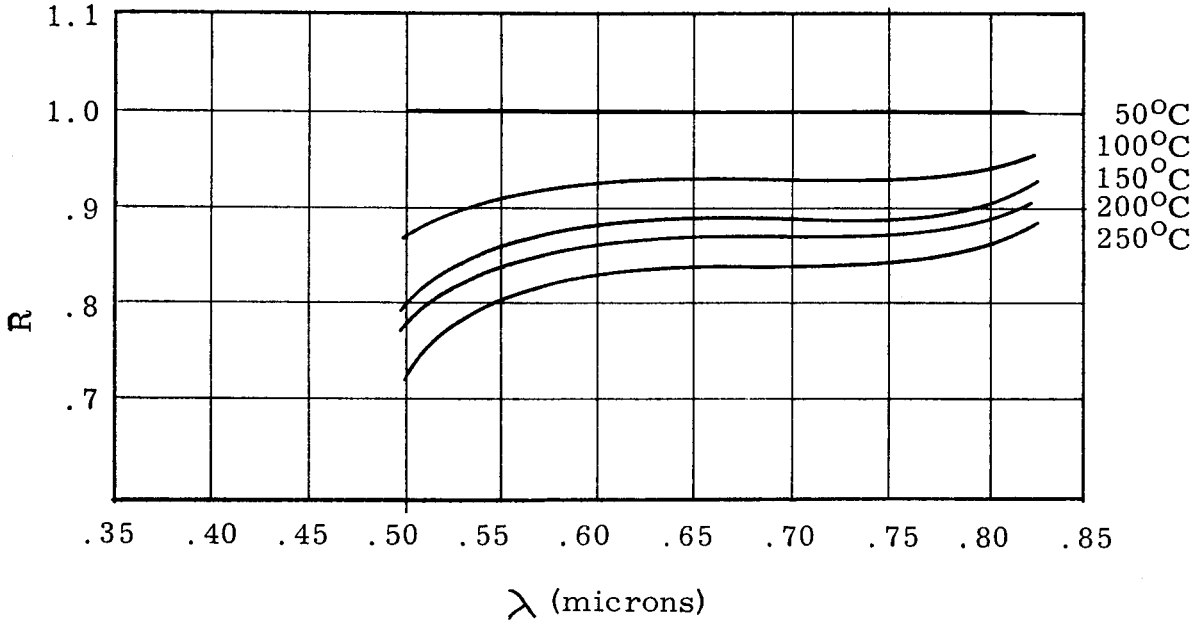

Fig. 18. Temperature Vs. Spectral Response

TABLE IX

Parameter Change at 200°C Storage Temp. Ti-Ag Front and Back Contacts

	Cell # 17-8	% Change	Cell # 19-6	% Change	Cell # 29-5	% Change	Avg. % Change
I_{sco}	27.2		26.0		25.7		
25	26.7	1.8	23.8	8.5	25.2	1.9	4.1
139	26.2	3.7	23.5	9.6	24.8	3.6	5.6
350	26.2	3.7	23.5	9.6	cell broken		6.6
950	26.0	8.1	23.3	10.4			9.2
V_{oco}	.870		.756		.890		
25	.860	1.2	.732	3.2	.890	0	2.2
139	.850	2.3	.736	2.6	.876	1.6	2.2
350	.850	2.3	.734	2.9	broken		2.6
950	.857	1.5	.756	0			.8
$P_{max\ o}$	15.5		8.8		16.2		
25	15.2	1.9	7.6	13.6	16.1	.6	5.4
139	14.8	4.5	7.4	15.9	15.4	4.9	8.4
350	14.7	5.2	7.4	15.9	broken		10.6
950	14.8	4.5	7.5	14.8			9.7

TABLE X

Parameter Change at 250° Storage Temp. Ti-Ag Front and Back Contacts

	Cell # 18-3	% Change	Cell # 18-4	% Change	Cell # 29-4	% Change	Cell # 16-8	% Change	Avg. % Change
I_{sco}	25.3		25.0		24.5		26.6		
25	25.1	.8	24.7	1.2	23.8	2.9	25.7	3.4	2.1
139	24.7	2.8	23.5	6.0	23.7	5.3	25.5	4.1	4.6
350	24.7	2.8	23.2	7.2	23.8	2.9	25.3	4.9	4.5
950	24.5	3.2	23.0	8.0	23.7	5.3	25.0	6.0	5.6
V_{oco}	.852		.810		.836		.868		
25	.852	0	.700	13.6	.824	1.4	.856	1.4	.7
139	.840	1.4	.400	50.6	.820	1.9	.820	5.5	2.2
350	.840	1.4	.350	56.8	.816	2.4	.808	6.9	2.7
950	.840	1.4	.340	58.0	.830	1.9	.808	6.9	2.6
$P_{max\ o}$	16.7		12.8		14.1		12.3		
25	14.1	15.6	7.0	45.3	12.6	10.6	11.7	4.9	7.8
139	14.1	15.6	2.4	81.3	12.4	12.1	10.6	13.8	10.4
350	13.9	16.8	2.1	83.6	12.2	13.5	10.0	18.7	12.3
950	14.3	14.4	2.1	83.6	12.4	12.1	10.2	17.1	10.9

Table XI

Parameter Change at 200°C Storage Temp. Ti-Ag Front and Sn-Ag Back Contacts

	Cell # 66-2	% Change	Cell # 67-4	% Change	Cell # 67-5	% Change	Avg. % Change
I_{sco}	19.8		19.6		22.9		
137 hrs.	19.3	-2.5	18.8	-4.1	21.7	-5.24	-3.9
323 hrs.	19.6	1.0	19.0	-3.0	22.2	-3.0	-2.3
V_{oco}	.890		.815		.850		
137 hrs.	.860	-3.4	.797	-2.2	.830	-2.4	-2.7
323 hrs.	.855	-3.9	.780	-4.2	.830	-2.3	-3.5
P_{max}	11.6		10.0		12.8		
137 hrs.	10.4	-10.3	9.1	-9.0	11.6	-9.4	-9.6
323 hrs.	10.3	-11.3	8.8	-12.0	11.9	-7.0	-10.1

Table XII

Parameter Change at 250°C Storage Temp. Ti-Ag Front and Sn-Ag Back Contacts

	Cell # 66-3	% Change	Cell # 66-7	% Change	Cell # 67-6	% Change	Cell # 67-8	% Change	Avg. % Change
I_{sco}	21.8		20.8		24.2		20.3		
137 hrs.	21.2	-2.8	20.3	-2.4	22.8	5.7	19.2	-5.4	-4.5
323 hrs.	21.4	-1.8	20.5	-1.4	23.1	-4.5	19.5	3.9	-2.9
V_{oco}	.915		.890		.890		.800		
137 hrs.	.875	-4.4	.860	-3.4	.860	-3.4	.780	-2.5	-3.4
323 hrs.	.850	-7.1	.847	-4.8	.847	-4.8	.775	-3.1	-4.9
P_{max}	15.2		12.0		16.3		10.5		
137 hrs.	13.3	-12.5	11.0	-8.3	15.4	-5.5	8.7	-17.0	-10.8
323 hrs.	12.9	-15.1	10.9	-9.1	14.6	-10.4	8.9	-15.2	-12.4

Table XIII

Parameter Change at 250°C Storage Temperature
2 x 2 cm Si solar cell. No solder

	Cell # S1	% Change	Cell # S2	% Change	Cell # S3	% Change	Cell # S4	% Change
$I_{sc(o)}$	114		116		112		118	
68 hrs.	112	1.4	114	1.2	114	1.4	116	1.1
235 hrs.	108	4.3	114	1.2	114	1.4	116	1.1
$V_{oc(o)}$	584		588		590		587	
68 hrs.	580	.7	585	.5	582	1.4	584	.5
235 hrs.	555	29	584	.7	588	.3	586	.2
$I_{.46(O)}$	100		106		103		100	
68 hrs.	88	12	101	4.7	98	4.8	98	2
235 hrs.	50	50	97	8.5	93	9.7	64	36

Table XIV

Parameter Change of Cells Having Sn-Ag Back and Ti-Ag Front Contacts

Cell #	Before Storage			After 137 Hours			After 323 Hours		
	R_S Ω	R_p Ω	Cmmf	R_S Ω	R_p Ω	Cmmf	R_S Ω	R_p Ω	Cmmf
66-2	.4	90	.070	.4	80	.070	.3	60	.0690
66-4	.4	670	.077	.2	700	.078	.3	260	.0753
*66-5	.5	320	.072	.4	310	.072			
*66-7	.4	120	.072	.2	90	.072	.3	70	.0720
67-4	.4	120	.055	.4	100	.053	.35	80	.0553
67-5	.4	240	.055	.4	170	.055			
*67-6	.4	4700	.052	.5	6900	.052	.31	230	.0538
*67-8	.4	200	.049	.3	130	.049			

*250°C storage
others 200°C storage
R_S - series resistance
R_p - shunt resistance
C - junction capacitance at V = O

Table XV

Percentage of Spectral Response Loss After 137 Hours of Storage

200°C Storage

	Cell #		
	66-2	67-4	67-5
Percent area lost after storage	5.3	4.6	4.1

250°C Storage

	Cell #			
	66-5	66-7	67-6	67-8
Percent area lost after storage	4.6	6.4	5.1	4.5

The relative spectral response curves taken at 0 and 137 hours show a decrease of response in the blue region. Figure 19 is a typical example. The percentage loss in the area under the curve was determined by planimeter measurements and is tabulated in Table XV. There is good correlation between the percentage of the area lost and the percentage of the short circuit current lost.

There were three other tests performed in this area. The first test consisted of cells which were chemically polished. After polishing (prior to diffusion) half the cells were stored at 250°C and half at room temperature for one week. After storage, the cells were processed normally and the electrical results compared. There was no difference observed between the two groups. The second test was conducted such that half of a group was stored at 250°C and the other half of the group was stored at room temperature for two weeks. In this case the cells were stored after the diffusion operation and then processed normally. Once again, a comparison showed no difference between the cells stored at 250°C and the cells stored at room temperature. The third test consisted of placing cells without an SiO anti-reflection coating in 250°C storage. The same degradation was seen for these cells as for the cells having an SiO coating. Attempts to reverse the degradation by the use of various surface clean-ups (HF, solvents, etc.) proved unsuccessful.

III. CONCLUSIONS AND RECOMMENDATIONS

From the results arrived at in the diffusion tests, it appears that in order to achieve any significant increase in conversion efficiency, techniques must be developed to fabricate cells having an extremely shallow diffused junction depth. It is believed that with the use of SiO_2 masking techniques the diffusion portion of the problem would present no serious technological difficulties. However, in order to obtain very shallow uniform junctions with the required degree of reliability, improvements must be made in the uniformity and crystallinity of the base material. Making contact to this thin diffused region may present some problems, but using "wrap around" fabrication techniques (GaAs "wrap around" solar cells have been fabricated), these problems should be relatively easy to solve.

It has been shown that the Sn-Ag ("N") and Ti-Ag ("P") contact mechanism, while it perhaps is not the ultimate, provides a cell with low series resistance and high strength contacts capable of high temperature operation. Although only one GaAs module has been fabricated, it was enough to determine that, using this contact in conjunction with the In-Ag-Pb high temperature

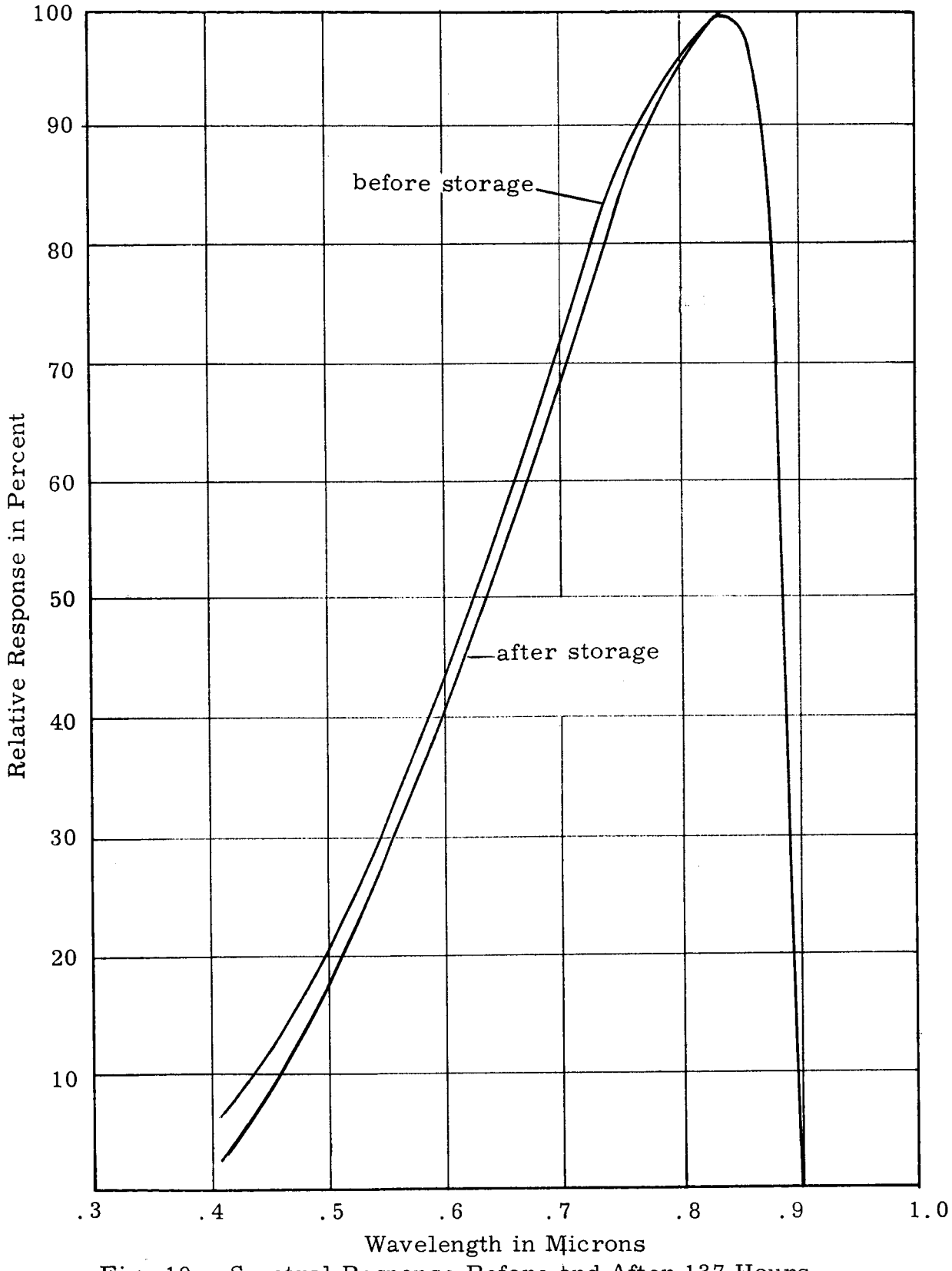

Fig. 19. Spectral Response Before and After 137 Hours of Storage at 200°C

solder, no serious problems would be encountered in modularizing the cells using the same techniques developed for fabricating Si solar cell modules.

Although the problem of electrical degradation during high temperature storage has not been solved, there has been much enlightening information obtained. It can be concluded that the junction is not physically changing and the contacts are not deteriorating during high temperature storage. It can also be concluded that the degradation is not inherent in the cell, since wafers heat treated at various points in the process yield the same electrical results as wafers which have not undergone high temperature storage. Degradation is observed only when the cells are stored at high temperature after the optimization etch step has been completed. There is also a decrease in parallel resistance, indicating that during high temperature storage a low resistance shunt is formed across the junction, probably at the edge of the cell. The above information when coupled with the decrease in the area under the spectral response curve suggests that the degradation problem is closely allied with the surface rather than the interior of the device. It is recommended that future work on the device include surface studies, incorporating surface passivation techniques.

Appendix A

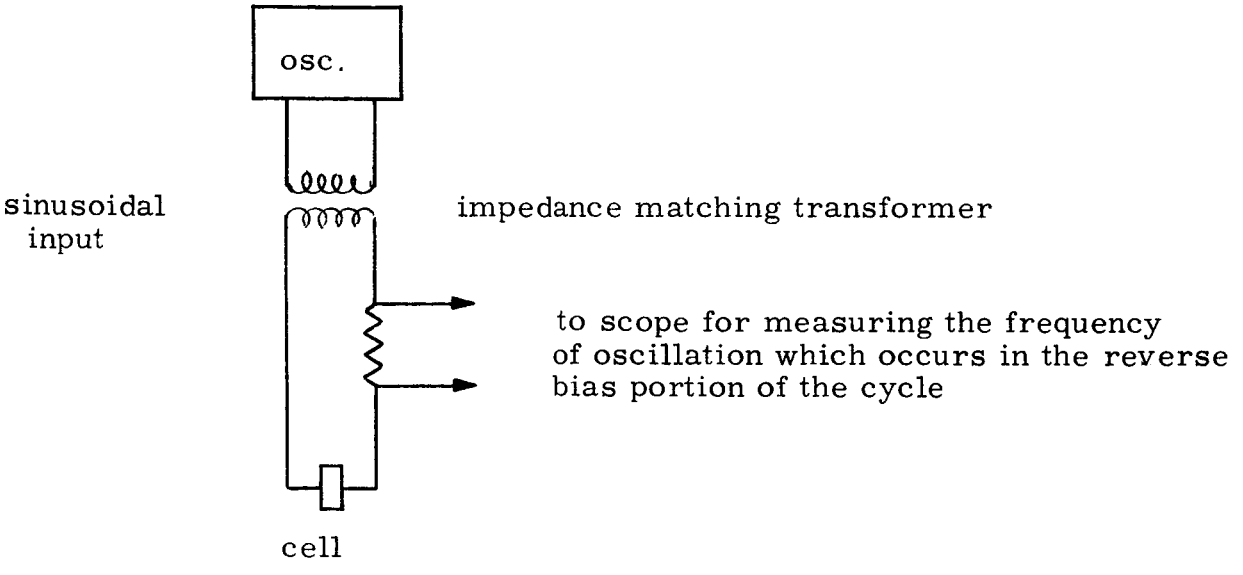

shape of output curve

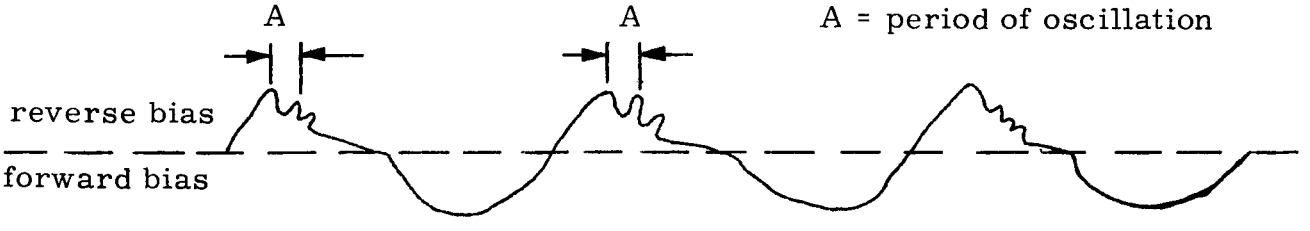

PERSONNEL

Engineers:

H. W. Kuzminski

F. J. McKendry

C. R. Oblinger

A. R. Topfer

Technicians:

W. C. Bartholomay

W. N. Henry